1985

Mississippi Lignite Utilization Stuides -- Task A, Experimental and Modeling Studies of Sulfur Release and Retention by Ash During Devolatilization and Combustion of Mississippi Lignite

W. E. Genetti

Open-File Report 85-1Fa

Mississippi Lignite Utilization Studies - Task A
Experimental and Modeling Studies of Sulfur Release and Retention by Ash During Devolatilization and Combustion of Mississippi Lignite

W. E. Genetti, Y. Y. Lee, and Frank W. Cox

1985

The Mississippi Mineral Resources Institute
University, Mississippi 38677

FINAL REPORT

TASK A OF GRANT FOR

MISSISSIPPI LIGNITE UTILIZATION STUDIES

TASK A: Experimental and Modeling Studies of $SO^{\wedge}$ Release and Retention By Ash During Devolatilization and Combustion of Mississippi Lignite

MMRI-85-1F
(G1144128)

Co-Principal Investigators

W.E. Genetti
Y.Y. Lee

Chemical Engineering Department
University of Mississippi
University, MS 38677

July 1985

ACKNOWLEDGMENTS

i

In addition to MMRI-85-1F, this work was supported by the Department of Chemical Engineering in the form of release time for the Principal Investigators, Mrs. Amy Burrow who provided a great deal of clerical support, and Mr. Arthur Bowles who helped us a great deal in the construction and maintenance of the equipment.

Mr. Frank W. Cox doctoral graduate student assistant, who was supported by the above grant, did the majority of the experimental and the modeling work on this project and is substantially responsible for producing this document.

ABSTRACT

Fluidized bed boilers fueled by coal are the subject of accelerating development in the U.S. and abroad. Combustion in a fluidized bed permits use of essentially all coals, including low-grade coals rich in ash and moisture such as lignite. Approximately thirty percent of our nation's 300 billion ton coal reserve is made up of lignite and Mississippi accounts for an estimated 8 billion tons. Due to strict environmental emission standards for sulfur dioxide, sulfur dioxide control in the combustors is very important. Limestone can be used in the bed to capture sulfur released by the combustion of the coal. The present investigation involves experimental and modeling studies which are aimed to contribute to the understanding of the mechanism of sulfur release and sulfur retention by ash in a fluidized bed coal combustor.

The objectives of this study were to show that Mississippi lignite would burn in a fluidized bed and to determine if the alkaline minerals in the ash would capture sulfur dioxide emitted by the burning liqnite. The experimental study revealed that sulfur was captured by the ash. The amount of capture depended on the operating conditions of the combustor. It was determined that limestone injection into the bed would be necessary to meet the environmental emission standards.

A pseudo steady-state mathematical model was developed for combustion of a porous single char particle that included both boundary layer and intra-particle reaction and diffusion characteristics. The model includes the energy equation as well as four species equations. This model is used to explain the trends of the sulfur capture with operating conditions of the fluidized bed combustor. The four gas species represented by the model are 0^, CO, CO2 and SO2. The SO2 species equation allows for the sulfur to exist as H2S, and COS in the char pores when a reducing environment exists. The sulfur gases are captured by CaO in the ash.

The results show that lignite char particles can exist in a fluidized bed combustor either in an ignited state or an unignited state depending on the

partides radius, bed temperature, and oxygen concentration. The model reveals SO^ ash retention trends for the effects of bed temperature and oxygen concentration for both ignited and unignited particles.

Comparison of emission data obtained early from our pilot size fluidized bed combustor has been made with the model trends. The model predicts trends for SO retention by lignite ash as a function of bulk stream 0^ concentration and bed temperature that are in agreement with the experimental emission data.

TABLE OF CONTENTS

LIST OF TABLES

LIST OF FIGURES

FIGURE PAGE

I. COAL PROPERTIES

1.1 ORIGINS

Coal was formed from partially decomposed plant debris which had collected in swamp lands. The swampy conditions prevented complete decay of the debris as it accumulated and eventually led to the material known as coal. This debris consisted of trees, ferns, rushes, lycopods, and several thousand plant species that have been identified in coal beds. Similar debris can be found in all types of coal but, the relative amounts vary considerably (1).

Coals are classified by their "type" and "rank". Coal type is determined by the nature of the plant material of which it originated. The microscopic study of coal and the relation of its different visible features to the original plant material forms the basis of coal petrography. Different coal types are composed of differing amounts of petrographic components called macerals (2) .

Macerals are combined into three main groups called vitrinite, exinite, and inertinite. Vitrinites are coalified woody tissues of leaves. Exinites are derived from resinous and waxy material of plants. Inertinites are

derived from charring of plant tissues (3). The average vitrinite content of American coals is in excess of seventy percent and their inertinite fraction is in the order of ten to fifteen percent. Exinite usually constitutes only a few percent, and the remaining material is inorganic mineral matter (2).

1.2 TYPE AND RANK

There are several methods used to describe coal megascopical ly. The two most often used methods are the Stopes system of lithotypes (8) and the Thiesson system of coal types (11). The lithotypes are defined in terms of four macroscopically different bands. Vitrain and Clarain are bright bands while Durain and Fusian are dull bands. Thiessen system of coal types divide banded bituminous coals into three coal types Bright, Semisplint and Splint. The nonbanded coals are divided into two coal types Cannel, and Boghead (3).

Rank is the most important property of coal and signifies the degree of maturation in the process of coal formation. The coal of lowest rank is lignite, followed in increasing rank by subbituminous coal, bituminous coal, and anthracite. Generally, the lower the coal rank, the lower the fixed carbon content and the lower the calorific value.

Also the moisture and volatile content increase as the rank decreases ¡(2). Approximately thirty percent of our nation's three hundred billion ton coal reserve is made up of lignite. Mississippi contains an estimated eight billion tons of lignite.

1.3 PROXIMATE AND ULTIMATE ANALYSIS

Coal is an extremely complex material. Nevertheless, with the rapidly expanding use of coal throughout the nineteenth century and the early part of the twentieth century, it became necessary to devise methods for coal analysis so that it could be possible to correlate coal compositon and coal properties with coal behavior.

The proximate analysis of coal may be considered as the determination of the moisture content, volatile matter content, ash content, and fixed carbon content (by difference) . Volative matter obtained during the pyrolysis of coal consists mainly of combustible gases such as hydrogen, carbon monoxide, methane plus other hydrocarbons; tar as well as incombustible gases such as carbon dioxide and steam. Ash is the residue derived from the mineral matter during complete incineration of the coal.

Ultimate analysis of coal is an absolute measure of the elemental composition of coal. Ultimate analysis expresses

the composition of coal in percentages of carbon, hydrogen, nitrogen, sulfur, oxygen, and ash (1).

1.4 SULFUR FORMS

The sulfur in coal has been considered in two classes; inorganic sulfur and organic sulfur. In the class of inorganic sulfur, two types of compounds are considered: the disulfides and the sulfates (4). Pyrite and marcasite are two disulfides with the same chemical form, FeS2« Pyrite is cubic whereas marcasite is orthorhombic. Since pyrite and marcasite are difficult to distinguish from one another all of the FeS2 is designated simply as pyrite. The organic sulfur is all the sulfur which is connected to the hydrocarbon matrix (1).

The total sulfur in coal varies in the range of two tenths to eleven weight percent (5) although in most cases it is between one and three weight percent.

Most of the information on organic sulfur is obtained by examination of the smaller molecular products which are obtained by breaking the organic coal matrix. The two methods most often used for breaking up the coal matrix are pyrolysis and hydrogenation. Both are very drastic methods, which change the structure of the coal and of the sulfur groups. Thiophenes and sulfides are the major components of tars from coal pyrolysis. Hydrogen sulfide and

the lower mercaptans and sulfides are found in the volatiles. Hydrogen sulfide and thiophenes are practically the only sulfur products of coal hydrogenation (18).

Attar estimates that thiophenes constitute forty to seventy percent of the organic sulfur in bituminous coals. The rest includes aryl sulfides, cyclic sulfides, and aliphatic sulfides at a ratio about three to two to one (18) . Disulfides and mercaptans may be present in lignites. Most of the sulfur in coal is pyritic with one-half to a third of the total sulfur being organic (4) . The sulfate sulfur is usually negligible. However, the amount of sulfate sulfur increase when the coal is exposed to air. It has been found that pyrite is readily air-oxidized to iron sulfates (6).

1.5 SULFUR ANALYSIS

Sulfur is an important consideration in coal utilization and, hence, there is a considerable amount of published work relating to the development of methods to improve the accuracy and precision of sulfur determination as well as improving the efficiency of the current techniques (1).

The three most widely used ASTM approved methods for total sulfur determination are the Eschka method, the bomb-

combustion method and the high-tempera ture combustion method. The most commonly used Eschka method involves combusting coal with one part of sodium carbonate and two parts of calcined magnesium carbonate. The sulfur compounds evolved as a result of the combustion react with the sodium carbonate and are retained as sodium sulfate. The solids are washed and reacted with barium chloride to form barium sulfate. The total sulfur can be calculated from the weight of the precipitated barium sulfate.

By the ASTM method sulfate sulfur is determined as the amount of sulfate ion soluble in dilute hydrochloric acid while pyrite is determined as the sulfur equivalent of the iron soluble in dilute nitric acid. The nitric acid extract is analyzed for iron, which is a more reliable measure of pyritic sulfur than sulfur itself. The organic sulfur is determined by difference from the data for total sulfur and sulfate plus pyrite sulfur (13).

Pyritic sulfur has also been determined by Mossbauer spectroscopy, scanning electron microscopy, and x-ray diffraction. Montano and Bommannaver used Mossbauer spectroscopy to study iron disulfide transformation to iron sulfate (10). Stewart and Whiteway used scanning electron microscopy to study the decomposition of pyrite during pyrolysis of coal (14) . Renton has shown that x-ray

diffraction when used for pyrite determination has a systematic relationship between lithotype and intensity response. For the same pyrite concentration you get a higher indicated pyrite concentration for vitrain than durain by x-ray diffraction (9). Gladfelter and Dickerhoof describe an improvement to the standard ASTM method for sulfur forms that include sulfide and sulfite sulfur present in hydrodesulfurized coal. The standard ASTM method does not analyze for sulfide and sulfite sulfur. When these forms are present in the coal the ASTM method gives incorrectly high values for organic sulfur (7).

1.6 MINERAL MATTER

”Mineral matter” in coal can be defined as discrete mineral grains, such as quartz or kaolinite, and all other elements except organically bound C,H,N,O, and S. The term "mineral matter" is often used interchangeably with "ash”. This is of course, incorrect since ash is actually the residue remaining after complete combustion of the organic portion of the coal matrix. Thus, the constituents of ash do not occur as such in coal but are formed as a result of chemical changes which take place in the mineral matter during the combustion process (3).

Several formulas have been proposed for calculating

the amount of mineral matter originally in the coal using the data from ashing techniques as the basis of the calculation. The Parr formula is widely used for this calculation :

Percent Mineral Matter = 1.08*A + 0.5*S

where A is the percentage of ash in the coal and S is the total sulfur in the coal (15).

Some common minerals found in coal are the clay minerals - illite, $KAl_2(AlSi_3O_{10})(OH)_2$, and kaolinite, $Al_4Si_4O_{10}(OH)_8$; sulfides - pyrite; carbonates - $CaCO_3$, $MgCO_3$; and oxides - hematite, Fe_2O_3 and quartz, SiO_2(16).

Minerals in coal occur as discrete grains or flakes in one of five physical modes:

- disseminated, tiny inclusions within macerals
- layers, horizontal planes
- nodules, spherical concretions
- fissures, fracture fillings

Thick layers and abundant nodules or rock fragments hamper mining operations, but are easily removed by standard coal preparation facilities. Disseminated minerals and the thinner layers are not removable by existing preparation facilities and mainly consists of mixtures of illite, quartz and pyrite (16).

Minerals can also be genetically classified according

to Mackowsky (17) as detrital, syngenetic, or epigenetic. Detrital minerals are those that were deposited in a coal forming peat swamp from slowly moving water or wind currents. Syngenetic minerals are those that formed within the peat during the early stages of its coalification. Under those conditions disseminated pyrite is thought to have formed in sulfate bearing peat by bacterial reduction of the sulfur. Much of this type of pyrite has a spherical form and is described as framboidal pyrite. Epigenetic minerals are mainly those found in fissures and void fillings. This class of minerals formed when they precipitated into joints that developed long after the peat had coalified. This probably occured during the late lignite or early subituminous stages of coalification (16).

1.7 MINERAL ANALYSIS

Three basic analytical technigues exist to evaluate the amount of mineral contained in coal:

- The high-temperature ash generated as part of the coal proximate analysis,
- The low-temperature ash produced by oxygen plasma oxidation,
- The mineral matter determined by optical point-count techniques.

The high-temperature ash is generated by combusting a weighted sample of coal in an oxygen-rich environment at 750 degrees Centigrade. Volatile portions of the ash are lost in this process. This loss is recognized and can be taken into account by the Parr formula (15). Chemical analysis can be performed on the ash and the original mineral content can be estimated.

The low-temperature ash is produced by radio frequency induced oxygen plasma oxidation at temperatures of 140 to 150 degrees Centigade. This removes the organic portion with minimal thermal effect upon the basic mineralogy (3). X-ray diffraction can be used for quantitative analysis of the minerals (16).

Mineral matter determined by optical point-count techniques uses density difference to separate the minerals for optical microscopic study and chemical analysis.

1.8 POROSITY AND SURFACE AREA

Coal is a porous material and is generally considered to consist of micropores having sizes up to approximately one hundred angstroms and macropores having sizes up to several thousand angstroms. Porosity appears to vary with carbon content. The macropores are usually predominant in the lower rank coals while higher rank coals contain

predominently micropores. Surface area of coal varies over the range ten to two hundred square meters per gram and tends to decrease with the increase in rank of the coal.

Porosity and surface area are two very important properties with respect to combustion of coal since the reactivity of coal increases as the porosity and surface area of the coal increases.

The porosity (total void volume of coal) can be determined from absolute density measurements made using helium and mercury as displacement fluids. Helium with its very small atomic diameter and its virtual lack of adsorption on coal is supposed to penetrate the entire pore structure. Mercury at normal pressures does not penetrate pores smaller than ten micrometers (36) . The Maximum pressure required to force mercury into a cylindrical pore of radius r is given by the Washburn equation (37), which simplifies to :

$$r=106/p$$

where p is in pounds per square inch and r is in microns. The pore distribution of coal can be determined by measuring the mercury displacement at different pressures. In order to get meaningful mercury densities of coals, it is essential to determine the minimum pressure needed to

fill the interparticle void volume (3).

The best known method for determining the specific area of porous solids is the BET (Brunawer, Emmett, and Teilor) gas adsorption method. The method first determines the number of molecules of gas, as a monolayer, which completely cover the surface of the solid. This valve multiplied by the cross-sectional area per molecule of the adsorbed gas then gives the surface area directly. In the BET method, gases normally are adsorbed near their boiling points to insure a monolayer coverage of the solid surface at elevated pressures of the gas. Both nitrogen and carbon dioxide have been used to determine the BET areas of coals. Carbon dioxide always results in higher BET areas than nitrogen (38).

II. COAL COMBUSTION

In direct combustion, coal is burned to convert the chemical energy of the coal into thermal energy. The thermal energy can then be used to make steam that can be used to turn a steam turbine to make electricity.

2.1 MECHANISM OF COAL COMBUSTION

During combustion, water and volatile material distill off first. Those volatiles burn outside the char particle. After devolatilization oxygen is able to diffuse to the char surface. Devolatilization occurs rapidly (.5-1 sec) compared to char combustion (100-300 sec) for particles of one millimeter size. Char consists of ash, carbon, sulfur and small amounts of hydrogen and oxygen. The overall reaction mechanism for a char particle is believed to be;

- Oxygen diffuses through the surrounding gas phase to the pores and reacts with the char carbon producing carbon monoxide,
- Carbon monoxide diffuses away from the particle and reacts with oxygen to produce carbon dioxide,
- Carbon dioxide diffuses away from the particle to the freestream and toward the particle to react with

the char carbon to produce more carbon monoxide.

Several experimental studies have helped us develop the overall char combustion mechanism. Phillips et al,(39) showed that the primary product of the oxidation of carbon above 1300 degrees Kelvin is carbon monoxide. Photographs of burning particles taken by Davis and Hottel (40) revealed at high temperatures the existence of a luminous zone around the burning particles. This is the zone where carbon monoxide is oxidized to carbon dioxide. Wicke and Wurzbacher (41) measured concentrations of oxygen, carbon monoxide, and carbon dioxide around burning carbon rods. They observed a maximum in the concentration profile of carbon dioxide near the rod surface at high temperatures.

Temperature measurements by Kish (42) showed a maximum in the temperature profile near the char surface. This temperature was considerably higher than the surface temperature of the particle. Smith and Gudmundson (43) revealed that the surface temperature of burning char particles is considerably higher than the ambient temperature. They also observed that the presence of water vapor causes the particles to burn hotter than those reacting in a dry atmosphere even though their reaction rates were lower. Kurylko and Essenhigh (44) performed a series of experiments with burning spheres of porous

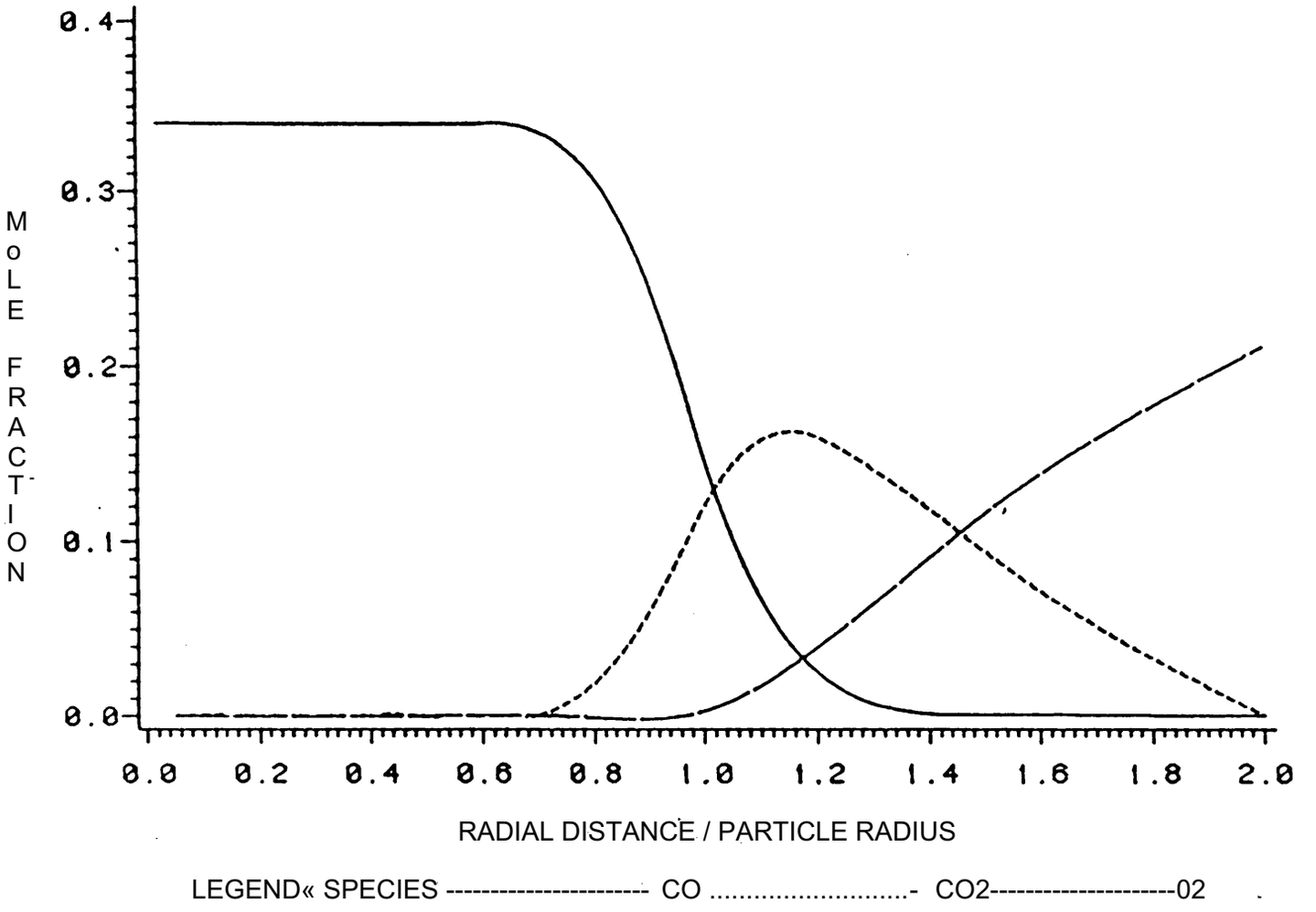

Figure 1. Burning Char Particle Species Profile

carbon. They observed temperature differences in the interior of the particle. Some temperature profiles in the interior of the particle showed a maximum, suggesting possible occurrence of the homogeneous reaction in the pores of the sphere. Figure 1 shows a schematic representation of a burning porous char particle.

2.2 COAL COMBUSTION CHEMISTRY

2.21 COMBUSTION OF VOLATILES

Devolatilization occurs first in the combustion of coal. These volatiles consist of hydrogen, carbon monoxide, hydrogen sulfide, methane, carbon dioxide, and vaporized tars. Since devolatilization occurs in about one-half to one second for a two millimeter particle in a fluidized bed, it is believed that these gases undergo combustion away from the char particle. These reactions can be represented by the following formulas:

$$H_2 + .\ 5O_2 + H_2O$$

$$CO + .5O_2 \quad CO_2$$

$$CH_4 + 2O_2 - CO_2 + 2H_2O$$

$$H_2S + 1.5O_2 \rightarrow SO_2 + H_2$$

2.22 RELEASE OF SULFUR DURING DEVOLATILIZATION

There is evidence that most of the original organic sulfur in some coals is released during devolatilization. Kruse and Shimp (31) concluded that a high percent of the organic sulfur of Illinois No. 5 and No. 6 coals was released during devolatilization. Moffat (22) showed that the major point of sulfur release for Texas and Louisiana lignite was during devolatilization. He concluded that this release was mainly derived from organic sulfur.

A fraction of the organic sulfur is released during devolatilization in most coals. In an investigation of the pyrolysis of Prince Coal, Brothers (45) noted that when ninety-five percent of the pyritic sulfur was removed prior to pyrolysis, the residual organic sulfur in the char decreased by fifty percent in comparison to that of char formed from the raw coal.

Stone et al. (46) showed that desulfurization is not tied directly to the devolatilization rate. While desulfurization may be tied to devolatilization, it is not the sole result of the act. The temperature range studied was 371 degrees Centigrade to 454 degrees Centigrade. Most of the sulfur removed in this study was from the organic form in the lignite. In general when coal is devolatilized the pyrite decomposes to pyrrhotite and hydrogen sulfide

and carbonyl sulfide is emitted.

$$FeS_2 + H_2 \rightarrow FeS + H_2S$$

$$FeS_2 + CO \rightarrow FeS + COS$$

Stewart and Whiteway (14) showed that pyrite decomposition to ferrous sulfide was virtually complete at devolatilization temperatures above 600 degrees Centigrade for coal from Nova Scotia.

Attar, Corcoran, and Gibson (34) suggest that gaseous hydrogen sulfide resulting from the decomposition of pyrite will react with unsaturated carbon molecules. It is believed that active carbon sites that are being generated simultaneously with the hydrogen sulfide during devolatilization could react with sulfur trapping it as newly formed and strongly bound "organic" sulfur. In Radio-Tracer work using ^{35}S-doped pyrite 38 percent of the overall sulfur liberated in the decomposition of the pyrite became fixed as "organic" sulfur (33) . Further evidence for the incorporation of sulfur as organic sulfur by trapping comes from the work of Cernic-Simic (47) who found a relation between the incorporation of sulphur, as organic sulfur, and coal rank; higher rank coals showing a smaller inclination for sulfur transfer. This was thought to be due to the chemical stability of high rank coals compared with lower rank coals.

Kruse and Shimp (31) found that iron appeared to control the amount of sulfur remaining in the char of Illinois coal after pyrolysis. The results are those expected if most of the organic sulfur in the coal is contained in the volatile products released during pyrolysis and if the sulfur from the pyrite is retained in the char.

It may be possible for the basic minerals in coal to capture sulfur during pyrolysis. The reaction of hydrogen sulfide with calcite, $CaCO_3$, is thermodynamically favorable at temperatures above 692 degrees Kelvin. However, devolatilization occurs very quickly for lignite in a fluidized bed combustor and probably very little capture by the basic minerals actually occurs during devolatilization. Calcium oxide will react with hydrogen sulfide faster than calcite, however, the calcite does not decompose very rapidly until temperatures around 800 degrees Centigrade are reached. By the time this temperature is reached devolatilization of the coal particles should be complete.

2.23 CHAR COMBUSTION

After devolatilization of the coal, char combustion begins. A two millimeter char particle will burn for one

hundred to three hundred seconds. Char combustion can be divided up into several reactions:

$$C_{+}.5O_2 \quad - \quad co \qquad RI$$

$$CO+.5O_2 \quad *^{co}2 \qquad R2$$

$$c+co_2 \quad * \quad 2CO \qquad R3$$

$$C+H_2O \quad + \quad CO+H_2 \qquad R4$$

$$CO \quad + \quad H_2O \quad +co_{2+}H_2 \qquad R5$$

$$^{H}2^{+} \quad '5O_2 \quad -H_20 \qquad R6$$

The char carbon is oxidized to carbon monoxide through reaction RI for a char particle that is reaction rate controlled. This carbon monoxide is oxidized to carbon dioxide in the homogeneous reaction R2. These two reactions are exothermic.

In a reducing environment the char carbon may "burn" in a carbon dioxide atmosphere by reaction R3 which is called the Boudouard reaction. This reaction is endothermic. Char carbon is burned in this manner when the particle combustion is diffusion controlled. Another endothermic reaction is the hydrolysis of the carbon by reaction R4.

Carbon monoxide will react with water to form carbon dioxide and hydrogen by reaction R5. This is the gas shift reaction, also called the water-gas shift reaction. This reaction is exothermic. Hydrogen is oxidized to water

by reaction R6.

2.24 SULFUR RELEASE AND CAPTURE DURING CHAR COMBUSTION

After devolatilization the primary forms of sulfur in the char should be ferrous sulfide and organic sulfur. The sulfur release during this stage of combustion can be represented by the following reactions:

$$FeS+1.5O_2 + FeO+SO_2 \quad S1$$

$$ORGANIC\text{-}S+O_2 - CO+SO_2 \quad S2$$

$$ORGANIC\text{-}S+CO_2 + CO+COS \quad S3$$

Burning of ferrous sulfide forms ferrous oxide and ferrous sulfate. About ten percent of the reaction product is ferrous sulfate at 400 degrees Centigrade. As the temperature is increased less ferrous sulfate is formed. At 700 degrees Centigrade and higher very little ferrous sulfate is formed and the reaction.proceeds as in reaction SI (35). Ferrous sulfide is very stable in a reducing environment and releases very little of its sulfur in practical temperature ranges (18).

Organic sulfur forms sulfur dioxide and carbon monoxide when it is reacted with oxygen as in reaction S2. In a reducing environment the organic sulfur may react with carbon dioxide to form carbonyl sulfide. Hydrogen sulfide and carbonyl sulfide can be related by the following

reversible reaction:

$$CO+H_2S \rightarrow COS+H_2$$

The reactions of the basic minerals with hydrogen sulfide, carbonyl sulfide, and sulfur dioxide are the major reasons for retention of sulfur in char during combustion. Calcium and magnesium oxides react with these gases and retain the sulfur in the form of sulfide or sulfate. The major retention reactions are:

$$MO + H_2S \quad + CaS + H_20 \qquad C1$$

$$MO + COS + CaS + C0_2 \qquad C2$$

$$MO + S0_2 + .5O_2 \quad + CaSO_4 \qquad C3$$

M is the alkali metals Ca or Mg. Reactions C1 and C2 have rate constants at least ten times smaller than C3. All three of the reactions are first order with respect to the sulfur species.

2.3 CONVENTIONAL COMBUSTION SYSTEMS

The combustion of coal involves burning in the presence of oxygen to produce heat. This heat can be used in boilers to produce steam. Over the years, several types of systems have evolved to accomplish this. These systems can be divided into slowly moving bed and entrained flow systems. Two common examples are the stoker-fired boiler and the pulverized-coal-fired boiler (1).

The underfeed stoker is an example of a slowly moving bed system. The underfeed stoker uses an auger to feed coal in the bottom of the boiler. The coal rises vertically in a retort and air enters through the side. The fire is ignited at the top and the flame front moves downward and its speed is matched by the rising flow of coal. Volatile matter from the coal mixes with the air and ignites as it passes through the incandescent top layer of the bed thereby effectively controlling smoke emissions (19). Stoker-fired boilers are used for many small-to-moderate capacity coal-fired boilers. Their size is usually limited to a steam capacity of 400-500 million Btu/Hr. It is the least complex to operate, because very little coal processing is needed (20).

An example of an entrained flow system is the pulverized coal-fired boiler. This system is used much more than the stoker-fired boilers. This mode of firing coal affords higher s team-generation capacity, is independent of the caking characteristics of the coal, and responds quickly to load changes (20). The pulverized coal-fired boilers use primary air to transport the coal to the burner. The primary air is usually 10 to 20 percent of the total combustion air. The remainder of the air needed for combustion is added in a manner to promote rapid

mixing. This air is called secondary air. In practice the velocity of the primary air-coal mixture is about 50 ft/sec to prevent flash back (19).

When burning high sulfur coals the pulverized coal-fired boilers and stoker-fired boilers must use a flue-gas-desulfurization system. This is necessary because the sulfur in the coal reacts with oxygen forming sulfur dioxide. The sulfur dioxide produced will react with oxygen and water in the atmosphere to yield sulfuric acid. This sulfuric acid is returned to the earth as acid rain. The current federal regulations require that SO_2 emissions must be limited to 1.2 lb of sulfur per million Btu of heat generated.

2.4 FLUIDIZED BED COMBUSTORS

2.41 HISTORY

In fluidized bed combustion, a bed of solid particles, such as sand, rests on a grate at the bottom of a boiler, and a blower is used to force air up through the grate at a velocity high enough to lift the particles and overcome their settling velocity. This grate is called the distributor. Crushed coal particles - normally in the millimeter size range - is fed into the boiler. The result

is a dense mixture of fuel and sand particles suspended in air. The burning particles account for less than 2 percent of the total weight of solids in the bed. The mixture has many of the physical properties of a fluid; for example, it has a pressure head, can flow around obstacles without mechanical agitation, and is exceptionally well mixed. The area of the boiler just above this bed of particles is called the "freeboard".

Fluidized beds have been used in the chemical industry since the early 1920's. The first large-scale, commercially significant use of fluidized beds was by Fritz Winkler for gasification of powdered coal. The first gas producer started smooth operation in 1926,to supply raw gas for synthetic chemical industries. Winkler gas generators were gradually replaced by generators which used petroleum feed stocks.

With war threatening in Europe and the Far East around 1940, chemical engineers in the United States developed the Fluid Catalytic Cracking process. This process used fluidized beds to promote contact of catalysts with feedstock for petroleum "cracking" reactions. In the metallurgical industry, fluidized beds have been used for improving ore-roasting techniques and more recently, for providing a uniform transfer of heat in various annealing

or surface-finishing processes.

The idea of using a fluidized bed to burn fuel was initially conceived in Europe in the 1920's, but it quickly disappeared. The concept was reinvented in England in the 1950's, but interest in nuclear power and cheap oil as sources of energy overshadowed the interest in coal and fluidized beds.

2.42 ADVANTAGES

The concept of fluidized bed combustion of coal offers two unique features that distinquish this technology from other methods. First, the particles of fuel and sand conduct heat with high efficiency. Direct contact between burning fuel and the other particles, and the components of a boiler, can yield a rate of heat transfer three to four times more efficient than the rate of transfer achieved through convection or radiation alone. The second advantage is that fluidized bed combustion offers unique opportunities for controlling pollution at its source- within the boiler itself.

The first advantage originally attracted attention in England. With improved rates of heat transfer, the size of a boiler can be substantially reduced. Also because of the turbulent mixing and the efficient transfer of heat,

temperatures within a fluidized bed are very uniform. Hot spots, which cause wear and tear on boiler parts, are avoided. The latent heat stored in the bed allows even wet or low-quality fuels to be burned smoothly and efficiently. The improved rates of heat transfer mean that fluidized beds can be operated at lower internal temperatures and still yield as much heat as conventional boilers. These lower temperatures are below the softening point of the coal ash which result in less problems in slagging and fouling of heat transfer surfaces.

It was the second advantage that accelerated interest in the United States. In the late 1960's, the U.S. Environmental Protection Agency (EPA) started some projects to test a new idea. By injecting limestone into the fluidized bed, along with coal, they believed they could have both a combustor and a chemical reactor. The coal would burn more efficiently because of the mixing properties of the bed and the limestone would react with sulfur dioxide forming ‹CaSO4. Limestone captures SO2 by means of the following reactions:

$$\text{‹CaCO3 (Iimestone} \rightarrow \text{) CaO + } C0_2$$

$$2SO_2 + 2CaO + 02\text{^ } 2CaSO_4$$

The first reaction, which is the calcining of limestone, is very endothermic. Ordinarily, this would be

an energy penalty on the system. However, the second reaction is exothermic and releases enough energy to replace the heat absorbed by the first reaction. The net result is a chemical system which is nearly thermoneutral.

Studies conducted with the fluidized bed boiler at Georgetown University showed a high degree of SO_2 removal between 85 and 95 percent. The Ca:S ratio used to achieve this high SO_2 removal was about 5.0 (21). Research by Modrak et al. (22) has shown that 90 percent SO_2 removal can be achieved with Ca:S ratios of 2.5-3.0 . The major reason for needing Ca:S ratios greater than 1.0 is that the molar volume of calcium sulfate is larger than that of calcium oxide. Therefore absorbed sulfur dioxide will block the pores preventing further sulfur dioxide capture in the pores.

Limestone capture of SO_2 reaches peak efficiency at 1,500 - 1,600 degrees Fahrenheit, which has become the standard operating range for most fluidized bed boilers. Boilers using conventional coal combustion techniques operate at 2,000 - 2,500 degrees Fahrenheit.

Operating fluidized beds at lower temperatures has an extra advantage in that it helps to reduce nitrogen oxide emissions. In combustion, nitrogen oxide is formed in two ways :

$$M2 + 0_2 \rightarrow 2N0$$

$$FUEL\text{-}N + 0_2 \; N\Theta$$

The first reaction is the oxidation of atmospheric nitrogen. The second reaction is the oxidation of nitrogen contained in the fuel. Molecular nitrogen in the atmosphere begins to oxidize at about 2,200 degrees Fahrenheit. Therefore, operating a fluidized bed combustor below 1,600 degrees Fahrenheit suppresses the atmospheric formation of nitrogen oxides that are produced in conventional coal boilers. Nitrogen oxide , however, is still formed by the second reaction in fluidized bed combustors.

2.43 FLUIDIZATION CHARACTERISTICS

As the flow rate of gas through a bed of solids is increased a limit is reached where the bed starts to expand and the particles become rearranged to offer a reduced flow resistance. When the gas flow rate is increased some more the particles separate and become freely supported in the gas. The superficial velocity at this point is called the minimum fluidization velocity. The pressure drop across the bed at minimum fluidization is equal to the total weight of the bed per unit distributor area.

When the gas velocity is further increased two

"phases" are formed: a dense or "emulsion" phase and a lean or "bubble" phase. The bubbling fluidized bed resembles a boiling liquid. The velocity at this point is called the bubbling velocity. For large particles of the size used in fluidized bed combustors the minimum fluidization velocity coincides with the bubbling velocity (23). Davidson and Harrison have based a two phase theory of fluidization on these two physical phases (24). Their basic assumptions are :

- the bed consists of an emulsion phase in which the gas flow rate is equal to the rate of minimum fluidization with the voidage fraction remaining essentially constant,
- the bubble phase carries the additional flow of fluidizing gas.

Results of a number of detailed experimental studies (25-29) support the two phase theory. Information is available on bubble formation, bubble rise velocity and on estimated values of the coefficient for mass exchange between the bubble and the surrounding emulsion phase (30).

The heat transfer coefficient h_t between the surface of a sphere of diameter d^ and a fluid through which it is moving with relative velocity u_Q is given by Ranz and Marshall (48) as:

$$Nu = h_t d / \kappa = 2 + \ddot{o}Pr^{/^}Re^{/2}.$$

The mass transfer coefficient K_d at the surface of a single sphere of diameter d_p moving with relative velocity u_Q through a fluid can be found from a similar equation by Froessling (49) as:

$$Sh=K_d d_p y/D= 2 + .6Sc^{1/3}Re^{1/2}.$$

2.5 SINGLE PARTICLE CHAR COMBUSTION MODELS

In general the combustion rate of a porous char particle is determined by both boundary layer and intraparticle reaction and diffusion characteristics. Most of the investigators of single particle combustion have developed models that isolate each problem so as to study it independently.

The boundary layer problem has been studied by either considering char particles impervious to diffusion or lumping all the intraparticle diffusion and reaction effects on the external surface of the particle. They also make assumptions about the rate of the homogeneous reaction and where it takes place.

Modeling efforts were started as early as 1923 (50). An isothermal single film model was proposed by Nusselt (51) who considered that the combustion of carbon particles was controlled by diffusion in the surrounding stagnant film, with the oxygen reacting with carbon to form CO and

CO- His model was extended by Burke and Schumann (52) , who also included the energy equation in the analysis. Burke and Schumann (53) also developed a double film model in which the carbon is consumed only by reacting with carbon dioxide produced at a flame sheet of carbon monoxide and oxygen, that is located at some distance from the surface of the particle. The double film model was modified by Spalding (54) , who proposed a smooth two-film model with all reactions in equilibrium. Van der Held (55) considered a flame of finite thickness instead of a flame sheet. Continuous models, with a finite rate of carbon monoxide oxidation everywhere in the system, were presented by Khitrin (56) and Hugo et al. (57). Hugo et al. attempted to explain theoretically the concentration profiles measured by Wicke and Wurzbacher (41).

The complete boundary layer problem was studied by Caram and Amundson (58) , Mon and Amundson (59,60,61) , and Sundaresan and Amundson (62,63,64) who used a hierarchy of models of varying complexity for their studies. Their extensive computations revealed some previously unsuspected features of the solution, such as the existence of up to five steady-states for some range of the model parameters. The transient boundary layer models revealed an interesting phenomena associated with the combustion of carbon

partides (64). They found particles undergo ignition for initial temperatures higher than a critical value and extinction after some conversion level. The effect of ambient conditions on the ignition and extinction phenomena were in qualitative agreement with the experimental evidence of Ubhayakar and Williams (65).

Most of the intraparticle models basically deal with the evolution of the char pore structure in the kinetically controlled regime. These refer mostly to the gasification of char by carbon dioxide. Gavalas (66) presented a model describing the intraparticle phenomena observed in the combustion of char particles. The intraparticle combustion problem was studied more fully by Srinivas and Amundson (67,68) using a simplified diffusion scheme and neglecting the intraparticle thermal gradients. A model for the transient combustion of porous carbon spheres including diffusion and reaction in the boundary layer was developed by Kurylko and Essenhigh (69). The model was employed in an attempt to explain experimentally observed behavior of burning spheres of carbon. Sotirches (70) studied the complete problem with use of pseudo steady-state model as well as transient models.

III. FLUIDIZED BED COMBUSTION EXPERIMENT

The purpose of the fluidized bed combustion experiments was to gather data on sulfur retention of Mississippi lignite ash during combustion with inert bed particles. Other studies (71) have shown that some coals release substantially lower amounts of sulfur dioxide when burned in a fluidized bed combustor compared to conventional combustion systems. The effects of operating conditions in the fluidized bed combustor on the retention of sulfur dioxide in Mississippi lignite ash were studied. This information was used to determine if limestone would be needed to meet the environmental performance standards for Mississippi lignite combustion in a fluidized bed.

3.1 COMBUSTOR DESIGN

The major parts of the fluidized-bed system used in this study are:

1. Combustion vessel
    A. Fluidized-bed portion
    B. Freeboard

C. Gas distributor

D. Cooling tubes

2. Lignite feeder

3. Air supply

4. Cyclone ash separator

5. Instrumentation

The combustion vessel is made from a six inch diameter schedule 40 stainless steel pipe. It is ten feet high and contains cooling tubes for bed temperature control. The distributor plate contains one hundred and thirty-seven holes one sixteenth inch in diameter. The bed height is about one and a half feet during fluidization. The area above the bed is called the freeboard.

The lignite is pulverized to about 8 mesh size (2.3mm) and feed by a screw auger type feeder. The feed hopper is pressurized with compressed air to prevent air back flow into the hopper. The lignite feed rate is adjusted by the gear setting from five pounds per hour to thirty pounds per hour.

The combustion air is supplied by a rotary positive displacement blower. The air flow rate can be determined by reading the pressure drop across an orifice with a monometer. The air velocity in the bed can be adjusted up to fourteen feet per second. The minimum fluidization

velocity in the bed is approximately four feet per second. The air is preheated by passing it through a heat exchanger with the hot flue gas.

A propane gas burner is positioned below the distributor plate. It is lighted during start-up to heat the bed before the lignite is fed. The air velocity in the bed is slowly raised simultanously with the gas flow rate until an air velocity of twelve feet per second is reached. At this time a small amount of lignite is fed through the overbed feeding system. This is done to prevent lignite accumulation in the bed during start-up. When the small amount of feed in the bed has dried and combustion starts the bed temperature will rise from about two hundred to about eight hundred degrees Fahrenheit. At this time the lignite feeder can be turned on and the feed rate adjusted. Bed temperatures for the study were in the range of twelve hundred to fifteen hundred and fifty degrees Fahrenheit. These temperatures were maintained by cooling with water tubes inside the bed. These temperatures were monitored with chrome 1-a lume 1 K-type thermocouples and indicators.

The flue gas is cleaned of particulate matter by a primary and secondary cyclone.

The sulfur dioxide emissions was monitored by a

Beckmann model 865 infrared analyzer with a 0 - 2,000 and a 0 - 10,000 parts per million range. The oxygen in the flue gas is monitored by a Thermco oxygen analyzer. Figure 2 shows a schematic diagram of the fluidized bed system.

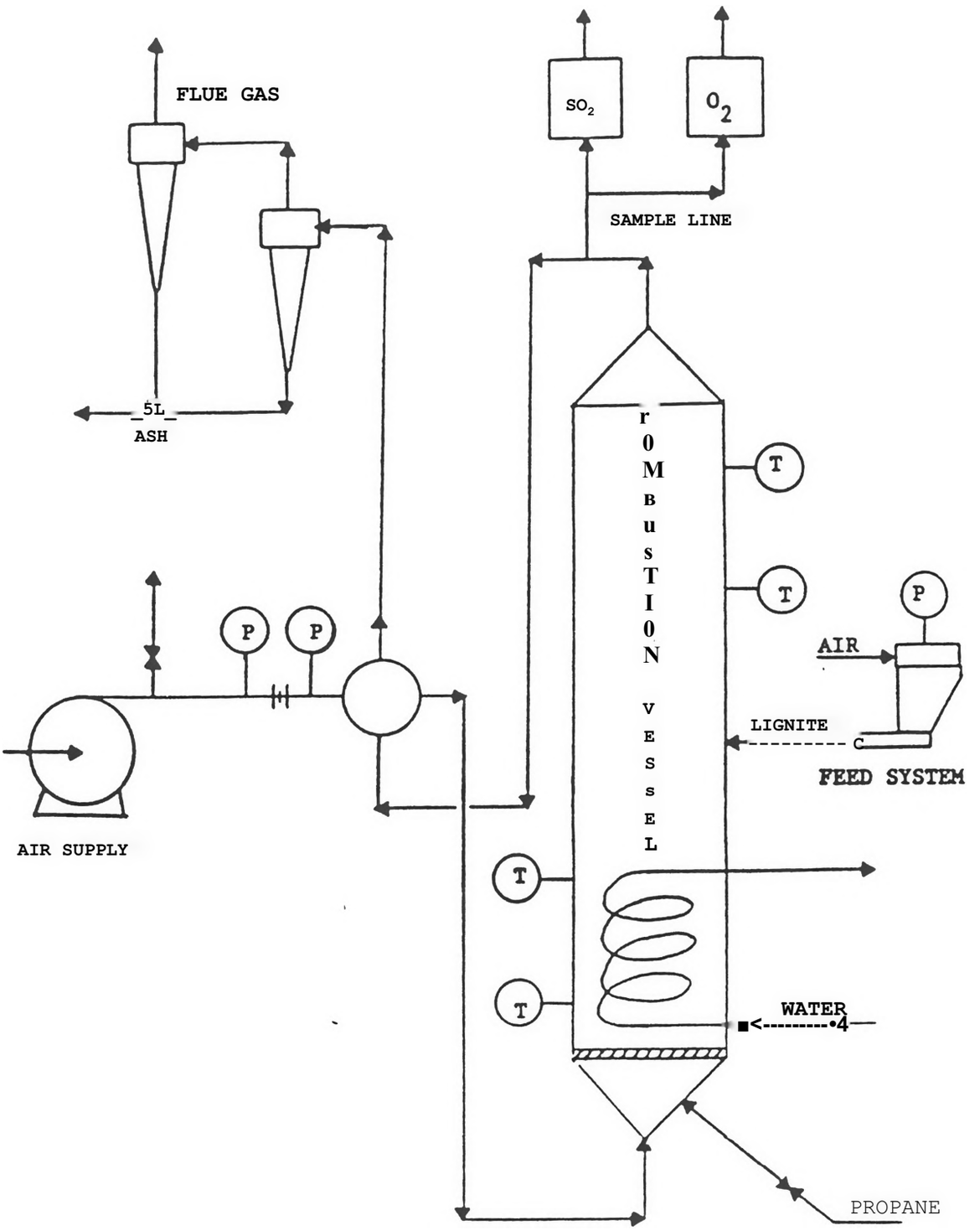

Figure 2. Fluidized Bed Combustor

3.2 LIGNITE ANALYSIS

Two types of Mississippi lignite were studied. We will call them type 1 and type 2. For type 1, about forty percent of the total sulfur was organic sulfur and sixty percent was pyritic sulfur. For type 2, ninety percent of the total sulfur was organic sulfur. Tables 1,2,3, and 4 show the ultimate analysis, mineral analysis, sulfur forms analysis, and proximate analysis for type 1 lignite. Tables 5,6,7, and 8 show the same analysis for type 2.

Table 1

Panola Mississippi Lignite Type 1

Ultimate Analysis

Species	Weight Percent
Carbon	56.41
Hydrogen	5.38
Nitrogen	0.6 3
Chlorine	0.01
Sulfur	2.74
Ash	19.85
Oxygen	14.98

Table 2

Panola Mississippi Lignite Type 1

Mineral Analysis

Species	Weight Percent
Phos. Pentoxide	0.01
Silica	42.89
Ferric Oxide	17.68
Alumina	16.03
Titania	1.40
Lime	7.75
Magnesia	1.34
Sulfur Trioxide	8.27
Potassium Oxide	0.27
Sodium Oxide	0.24

Table 3

Panola Mississippi Lignite Type 1

Sulfur Forms

Sulfur Type	Weight Percent
Pyritic Sulfur	1.66
Sulfate Sulfur	0.03
Organic Sulfur	1.05
Total Sulfur	2.74

Table 4

Panola Mississippi Lignite Type 1

Proximate Analysis

Substance	Weight Percent
Water	40
Volatile Matter	36
Fixed Carbon	12
Ash	12

Table 5

Panola Mississippi Lignite Type 2

Ultimate Analysis

Species	Weight Percent
Carbon	46.71
Hydrogen	4.19
Nitrogen	0.61
Chlorine	0.07
Sulfur	0.59
Ash	31.84
Oxygen	15.99

Table 6

Panola Mississippi Lignite Type 2

Mineral Analysis

Species	Weight Percent
Phos. Pentoxide	0.05
Silica	76.77
Ferric Oxide	3.66
Alumina	7.12
Titania	2.08
Lime	2.80
Magnesia	0.52
Sulfur Trioxide	3.02
Potassium Oxide	0.38
Sodium Oxide	0.11

Table 7

Panola Mississippi Lignite Type 2

Sulfur Forms

-Sulfur Type	Weight Percent
Pyritic Sulfur	0.01
Sulfate Sulfur	0.06
Organic Sulfur	0.52
Total Sulfur	0.59

Table 8

Panola Mississippi Lignite Type 2

Proximate Analysis

Substance	Weight Percent
Water	24
Volatile Matter	40
Fixed Carbon	14
Ash	22

3.3 GENERAL OBSERVATIONS

All of the experiments performed in this study used an overbed feed system. Since the alumina bed particles were approximately the same size as the lignite particles (2-3mm), the difference in density of the particles caused different fluidization characteristics resulting in the lignite particles burning at the top of the bed in about a a four inch layer. This minimized contact of the lignite particles with sulfur released by other particles in the bed. The residence time of the released sulfur in the bed of the burning particles was very small compared to the sulfur capture rate of alkaline minerals in the lignite ash. The trends observed from this study should correspond to those expected from sulfur capture in the ash during char combustion of individual particles. The majority of sulfur captured by each particle should be sulfur that originated from the particle. Most of the volatiles were released and burned in the freeboard. The sulfur that leaves the particles in this stage of combustion have very little chance of being captured by other particles, since the volatile burning occurred away from the particles above the bed.

By using inert bed particles approximately 20 mesh

size (. 8 3 3 mm) the lignite particles will mix well vertically through out the bed. By using underbed feeding the volatiles will burn in the bed.

The experimental runs usually lasted about an hour and a half. At this time the furnace would be cooled down and the ash was separated from the alumina particles in preparation for another run. Very little ash was found in the cyclone after each run. The majority of the ash was found in the bed. This observation seemed to indicate that the Mississippi lignite was a reducing density type coal. The ash particles did not reduce in size enough to be blown through the freeboard to the cyclone separators.

If the runs lasted long enough the char particle and ash density in the bed would become great enough that ash agglomeration would occur in the bed. Ash agglomeration causes the bed temperature to fluctuate and eventually leads to extinction of the combusting particles in the bed. Usually the runs did not last long enough for this to occur. Also, care had to be taken during the start-up period to prevent ash agglomeration. If lignite was fed on top of the bed before it was fluidized the particles would come in contact causing agglomeration.

3.4 EXPERIMENTAL RESULTS

The composition of sulfur dioxide measured in the flue gas of the fluidized bed combustor while burning type 1 Mississippi lignite is shown in figure 3. This figure shows the concentration of sulfur dioxide in parts per million plotted against bed temperature in degrees Fahrenheit. Curves are plotted for oxygen compositions of 9, 9.5, 10, 11, and 13 percent. The curves are all similar with a minimum at about 1000 degrees Kelvin.

This data is used to calculate the fraction of sulfur being retained by the ash. Type one Panola Mississippi lignite can be represented by the following molecular formula:

$$^{CH}1.445°0.199^{S}0.0182$$

Material balances can be written for combustion with excess air. These balances will indicate the sulfur dioxide concentration to be expected in the flue gas if all of the sulfur in the lignite was released. The fraction of sulfur retained is calculated by subtracting the ratio, of measured sulfur dioxide concentration to calculated sulfur dioxide concentration, from one.

A Plot of sulfur retained versus bed temperature for an oxygen concentration of 13 percent in the flue gas is

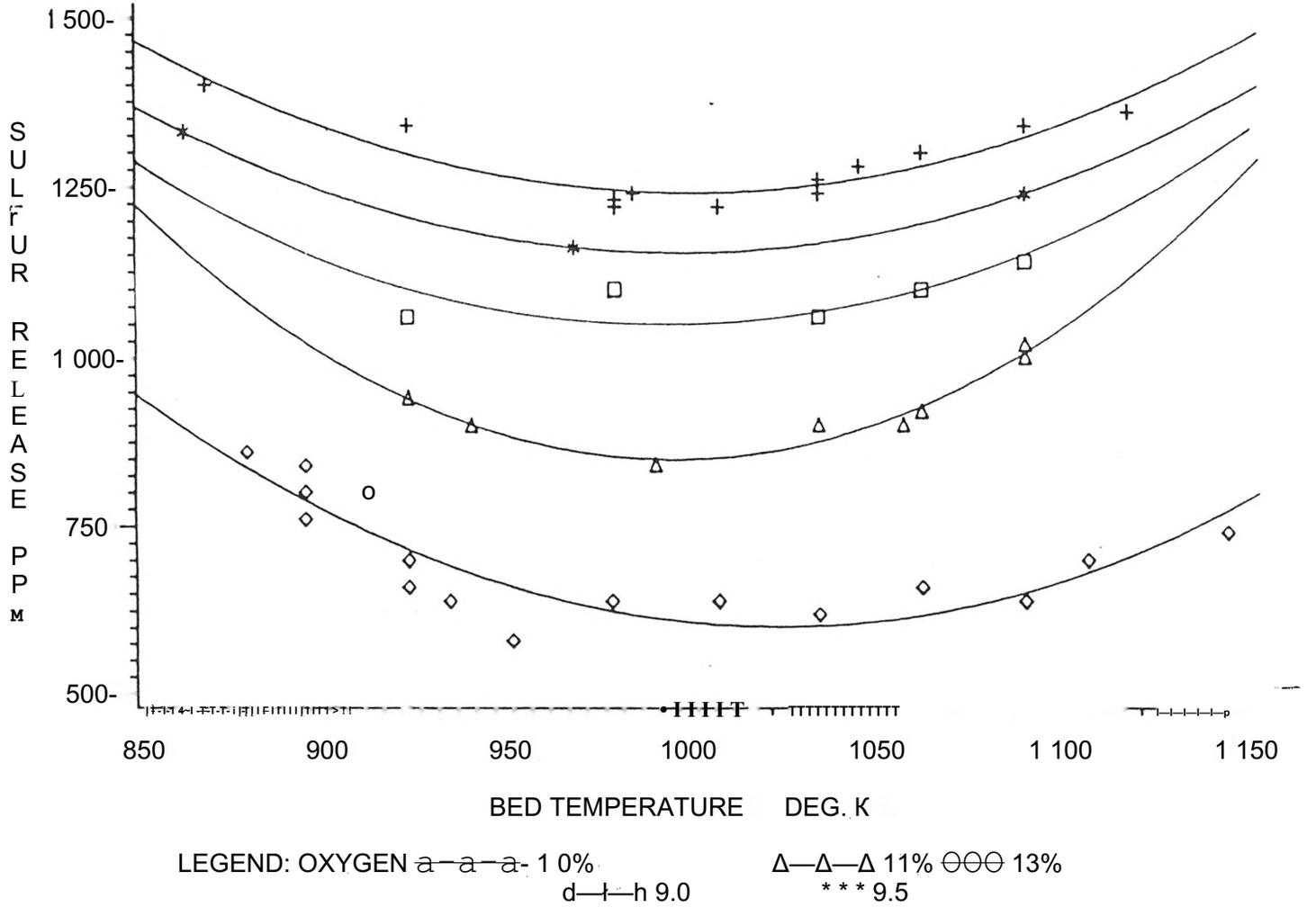

Figure 3. Sulfur Release vs. Bed Temperature

given in figure 4. The data appears to reach a maximum of 39% sulfur retained between 1000 and 1020 degrees Kelvin.

A plot of sulfur retained versus bed temperature for an oxygen concentration of 11 percent in the flue gas is given in figure 5. The data appears to reach a maximum of 33% sulfur retained between 980 and 1000 degrees Kelvin.

A plot of sulfur retained versus bed temperature for an oxygen concentration of 9 percent in the flue gas is given in figure 6. The data appears to reach a maximum of 20% sulfur retained between 980 and 1000 degrees Kelvin.

A plot of sulfur retained versus oxygen compos ition in the flue gas for temperatures of 978 degrees Kelvin and 1089 degrees Kelvin are shown in figure 7. The data noted by ▲ may be incorrect. We did not prove that the lignite for this run had the same properties. However, the lignite for this run was from the same source. The fraction of sulfur captured appears to level off at about 39 percent at a flue gas oxygen compositions of 14 percent and greater.

Type two Panola Mississippi lignite can be represented by the following molecular formula:

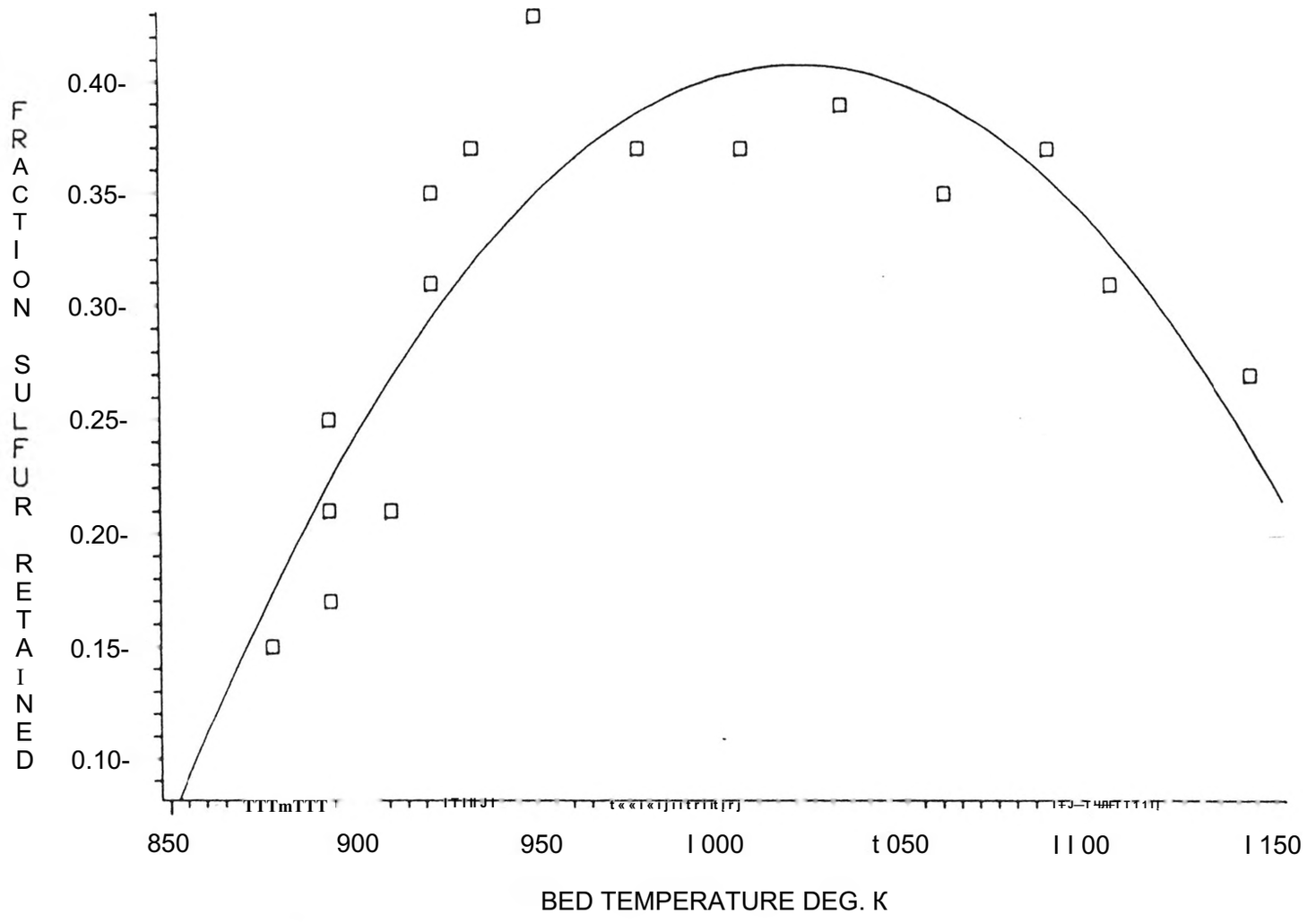

Figure 4. Sulfur Retained vs. Bed Temperature, = 130 $_2$

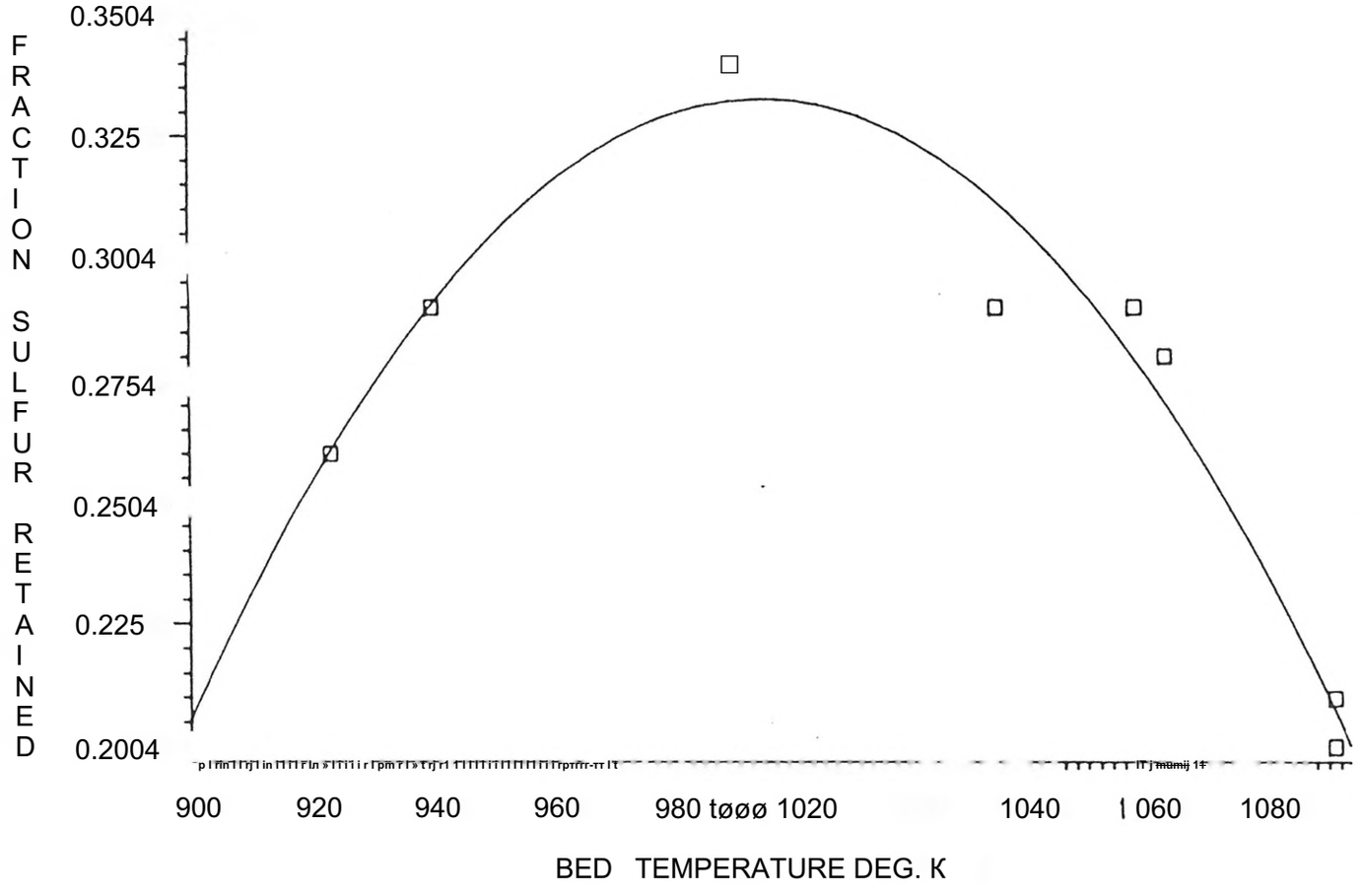

Figure 5. Sulfur Retained vs. Bed Temperature, O_2 = 11%

en
NJ

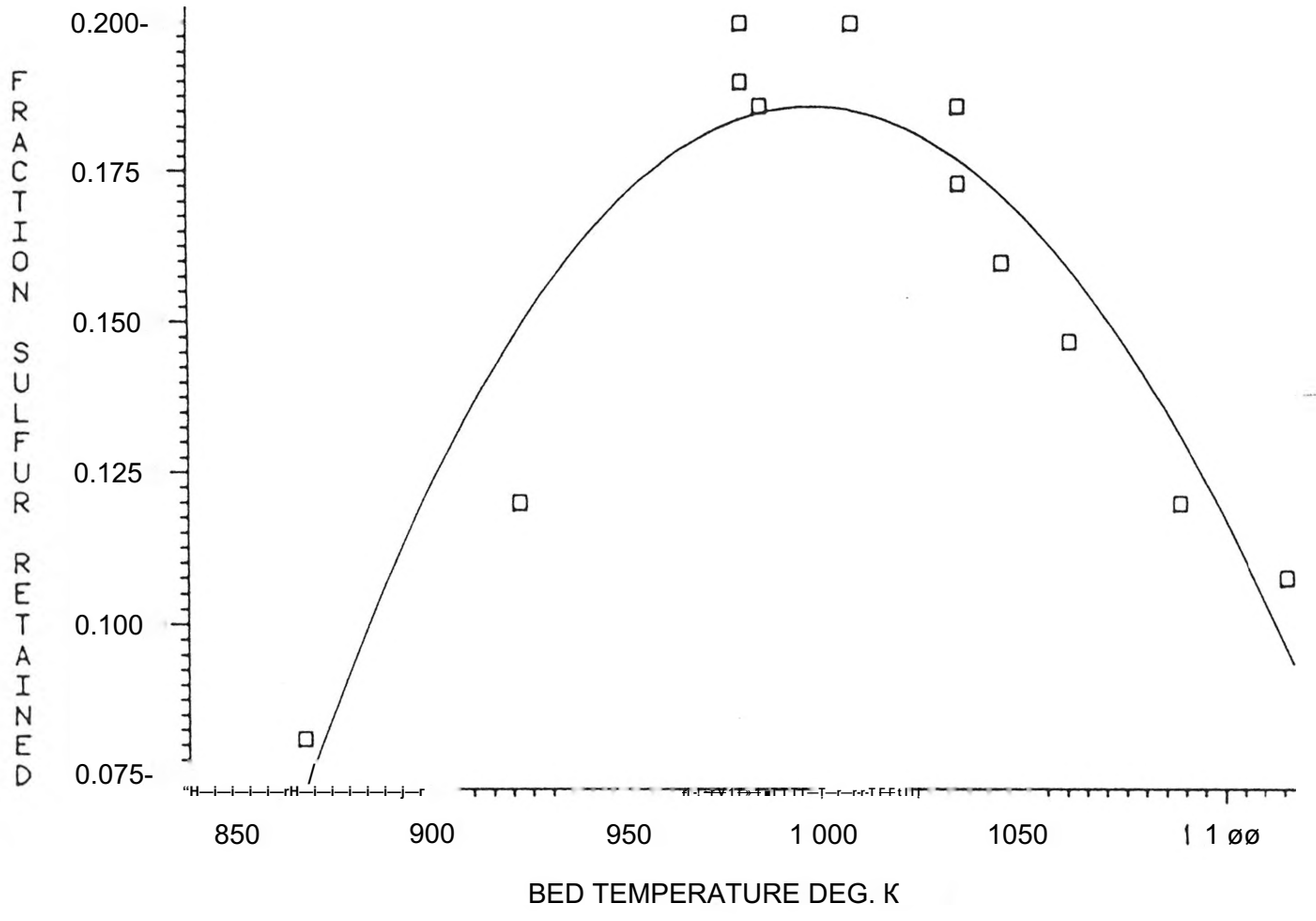

Figure 6. Sulfur Retained vs. Bed Temperature, 0_2 = 9%

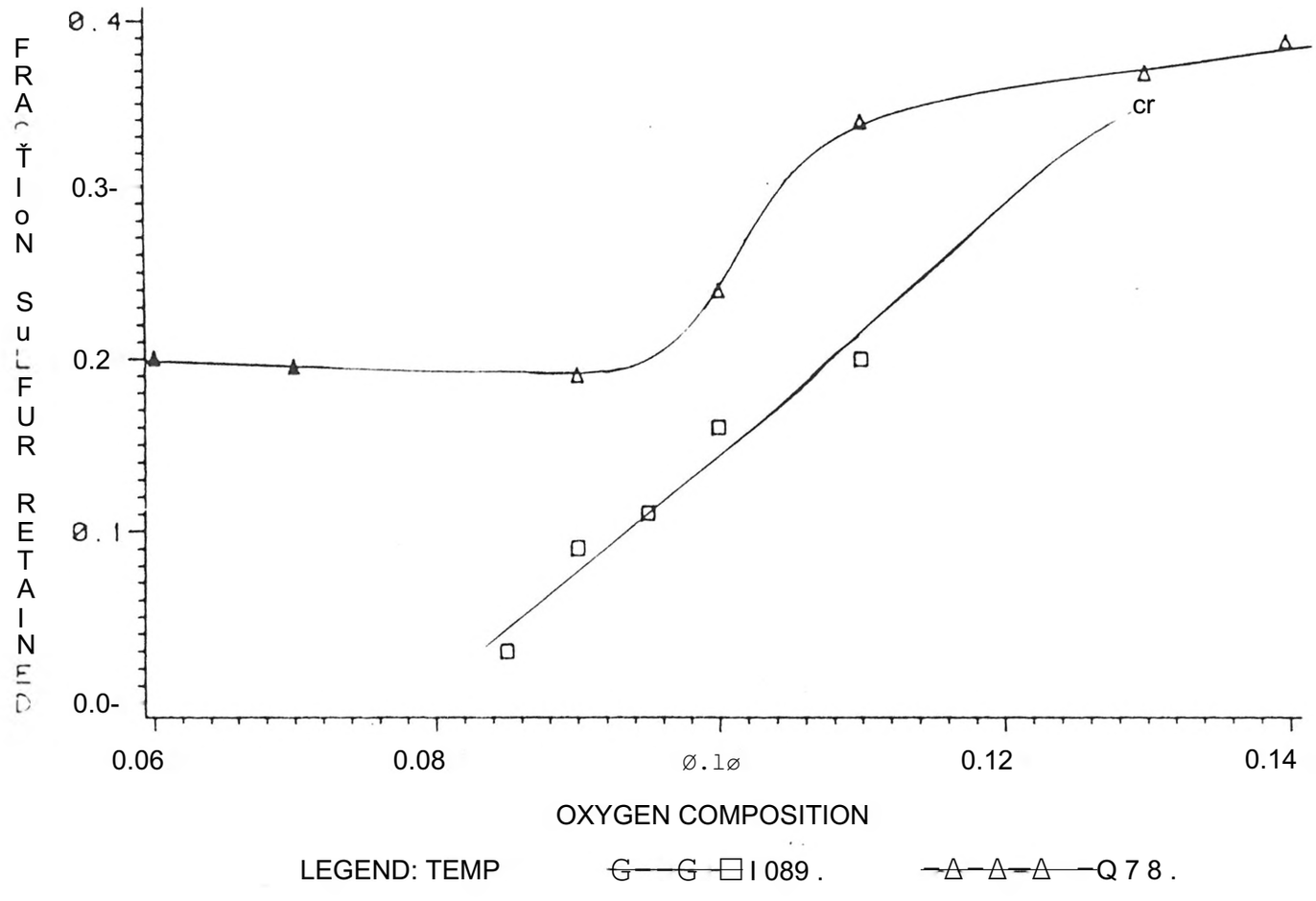

Figure 7. Sulfur Retained vs. Oxygen Composition

$^{H}1.076^0.2566^0.004727

This lignite has lower amounts of sulfur, but ninety percent of it is organic sulfur. Only forty percent of the sulfur in type one Panola Mississippi lignite was organic. The (Ca + Mg) :S ratio for type one lignite is 0.4. This ratio is 1.11 for type two lignite. This seems to indicate a higher potential for sulfur capture in type 2 lignite.

We observed between 260 to 280 parts per million sulfur dioxide emissions for thirteen percent oxygen composition in the flue gas for type two Panola Mississippi lignite. The amount calculated that we would expect to observe if all the sulfur was emitted is 285 parts per million.

We observed between 375 to 410 parts per million sulfur dioxide emissions for ten percent oxygen composition in the flue gas for type two Panola Mississippi lignite. The amount calculated that we would expect to observe if all the sulfur was emitted is 392.

These results show that even though the (Ca+Mg) :S ratio is higher for type two Mississippi lignite (as compared to type one) we have very little capture. Perhaps, most of the original organic sulfur in Mississippi lignite is released during devolatization and this sulfur is not captured during this period. Since type two Mississippi

lignite has very little pyritic sulfur we would not expect much sulfur capture.

The experimental results indicate that the optimum bed temperature for sulfur capture appears to be about 1000 degrees Kelvin. The amount of sulfur retained increases with increase in excess oxygen. For normal industrial operating conditions the excess oxygen is 20 percent which corresponds to 4 percent oxygen in the flue gas. At these conditions negligible sulfur will be retained by the ash and limestone will be needed to reduce sulfur emissions to environmentally acceptable levels. For the lignite studied 77 percent of the sulfur must be removed from the gas stream. This can be achieved by adding approximately 10 pounds of limestone per 100 pounds of lignite to the bed.

IV. SINGLE PARTICLE CHAR COMBUSTION MODEL

4.1 DEVELOPMENT OF MODEL

A pseudo steady-state model was developed for combustion of a porous single char particle that included both boundary layer and intra-particle reaction and diffusion characteristics. The model consists of a spherical char particle, with conical pores, surrounded by a boundary layer. This boundary layer thickness is determined by using the Nusselt Number calculated for a sphere of diameter, d_p, with fluid flowing at a relative velocity, U_o, around it. The expression given by Ranz and Marshall (3) for the Nusselt Number is:

$$Nu_p = 2 + 0.6\ Re_p^{1/2}\ Pr^{1/3} \qquad (1)$$

The distance r_f from the center of the particle to the outer edge of the boundary layer is calculated from Equation 2

$$r_f = \frac{Nu_p\ (r_p)}{(2 - Nu_p)} \qquad (2)$$

This equation is calculated by assuming an effective stagnant boundary layer for a given Nusselt Number. It is derived in Appendix A. The combustion reactions used in the model are:

$$C + 1/2O_2 \longrightarrow CO \quad \text{Exothermic}$$

$$CO + 1/2O_2 \longrightarrow CO_2 \quad \text{Exothermic}$$

$$CO_2 + C \longrightarrow 2CO \quad \text{Endothermic}$$

The char carbon is oxidized to CO through the first reaction for a char particle that is reaction rate controlled. The CO is oxidized to CO_2 by the second reaction. These reactions are exothermic.

In a reducing environment the char carbon may "burn" in a carbon dioxide atmosphere by the Boudouard reaction which is endothermic.

Sulfur is released in the model by oxidation of ferrous sulfide and organic sulfur with O_2 to form SO_2. The organic sulfur is also released in the model by reaction with CO to form carbonyl sulfide. These reactions are:

$$FeS + 3/2\ O_2 \text{ ------} > SO_2 + FeO$$

$$(Organic)\ S + O_2 \text{ -----} > CO + SO_2$$

$$(Organic)\ S + CO_2 \text{ -----} > CO + COS$$

In a reducing environment which may exist in the pores the sulfur containing gases will exist as H_2S or COS. In an oxidizing environment the sulfur containing gas will be SO_2.

Sulfur is captured in the model by the three reactions:

$$SO_2 + 1/2\ O_2 + CaO \text{ ------} > CaSO_4$$

$$H_2S + CaO \text{ -----} > H_2O + CaS$$

$$COS + CaO \text{ -----} > CO_2 + CaS$$

Sulfur dioxide can react with CaO to form $CaSO_4$, H_2S can react with CaO to form CaS, and carbonyl sulfide may react with CaO to form CaS. In the analysis the assumption is made that all $CaCO_3$ initially in the ash has been calcined to CaO during pyrolysis. This is a good assumption for particle temperatures greater than 800°C.

4.2 MATHEMATICAL FORMULATION

The char model differential equations are developed by mass and energy balances about a spherical shell of thickness dr.

The energy equation can be written in the form:

Energy conducted in + Energy convected in + Heat generated within = change in internal Energy + Energy conducted out + Energy convected out

If we use spherical coordinates and assume heat transfer only in the r direction the energy quantities are given as follows :

$$\text{Energy conducted in} = -k \frac{\partial T}{\partial r} r^2 4\pi$$

$$\text{Energy convected in} = \sum_{i=1}^{4} N_i \bar{C}_p (T-T^\circ) 4\pi r^2$$

$$\text{Net molar flux} = N_i = (C_i \bar{U} - V_i \frac{\partial C_i}{\partial r})$$

$$\text{Energy conducted out} = -k \frac{\partial T}{\partial r} r^2 4\pi - \frac{\partial}{\partial r} (4\pi \kappa r^2 \frac{\partial T_x}{\partial r}) dr$$

$$\text{Energy convected out} = \sum_{i=1}^{4} N_i \bar{C}_p (T-T^\circ) 4\pi r^2 + \frac{\partial}{\partial r} \left(\sum_{i=1}^{4} N_i \bar{C}_p (T-T^\circ) 4\pi r^2 \right) dr$$

$$\text{Heat generated within} = R_h (-\Delta H_h) V_p + s' s' A_p$$

Change in internal Energy = 0 for steady-state

where: $V_p = \Theta 4\pi r^2 dr$ = pore volume of spherical shell

$A_p = 2\pi\alpha / 1 + a N^2 dr$ = Pore area of spherical shell for conical pores

N = number of pores = $4\theta/\alpha^2$, see appendix B

r = distance from char particle center

Θ = pore volume/total volume

$a = \frac{r}{r_c}$ = radius of pore/radius of char (see appendix B)

$R_\wedge$ = homogeneous reaction rates

$R_\$$ = heterogeneous reaction rates

ΔH_L = heat of homogeneous reactions

$\Delta H_\$$ = heat of heterogeneous reactions

T = temperature

T_o = reference temperatures

$\bar{C}_p$ = specific heat

C_i = species i concentration

i = 1, 2, 3, 4 for O_2, CO_2, CO, SO_2

$\bar{U}$ = convective flux velocity

$\mathcal{D}_i$ = diffusivity of species i

κ = thermal conductivity

Combining the relations above gives:

$$-\kappa \frac{\partial T}{\partial r} 4\pi + \sum_{i=1}^{4} N_i \bar{C}_{p_i} (T-T_o) 4\pi r^2 + R_n (-\Delta H)_n \Theta 4\pi r^2 dr$$

$$+ R_s (-\Delta H)_s 2\pi (4\sigma r) \int_a^1 dr = -k \frac{\partial T}{\partial r} 4\pi r^2 - (k_r \nabla T) 4\pi r^2 dr$$

$$+ \sum_{i=1}^{4} N_i C_{p_i} (T - T_o) 4\pi r^2 + \int_{3r}^{2a} \left(\sum_{i=1}^{4} N_i C_{p_i} (T-T_o) 4\pi r^2 \right) dr$$

This reduces to the final form of the energy differential equation:

$$R_h\,(-\Delta H)\,\theta\,r^2 + R_s\,(-\Delta H_s)\,2\Theta\,r\,\frac{\sqrt{1+\alpha^2}}{a} \qquad (1)$$

$$\frac{\partial}{\partial r} = k\frac{\partial T}{\partial r} + \sum_{i=1}^{4} N_i C_{pi} (T - T^\circ)\, r^2)$$

The chemical species equation can be written in the form:

Diffusion in + Convection in + Generation

= Accumulation + Diffusion out + Convection out

If we use spherical coordinates and assume transport only in the r direction the species equation quantities are given as follows:

$$\text{Diffusion in} = A_i r^2 \left(-P_i \frac{\partial C_i}{\partial r}\right)\theta$$

$$\text{Convection in} = 4\pi r^2 (C_i U)\theta$$

$$\text{Diffusion out} = 4\pi\theta r^2 \left(-P_T \cdot \tau_{r\theta}\right) + 4\theta\pi \frac{\partial}{\partial r}\left(-r^2 V_i \frac{\partial C_i}{\partial r}\right) dr$$

$$\text{Generation} = R_i\, 4\pi\theta\, r\, dr + R_i\, 2\pi N_s a r \sqrt{1+a^2}\, dr$$

Accumulation = 0 for steady-state

Combining the relations above gives:

$$4\pi\theta r^2 \left(D_i \frac{\partial C_i}{\partial r}\right) + 4\pi\theta \frac{\partial}{\partial r}(C_i U) + R_i\, 4\pi\theta\, r\, dr + R_s\, 2\pi\theta \sqrt{1+a^2}\, r\, dr$$

$$= 4\pi\theta r^2 \left(D_i \frac{\partial C_i}{\partial r}\right) + 4\pi\theta \frac{\partial}{\partial r}\left(-r^2 P_i \frac{\partial C_i}{\partial r}\right) dr + 4\pi\theta \frac{\partial}{\partial t}(C_i U)$$

$$+ 4\pi\theta \frac{\partial}{\partial r}(r^2 C_i U)\, dr$$

This reduces to the final form of the species differential equation:

$$\frac{\partial C_i}{\partial t} + \frac{1}{r^2}\frac{\partial}{\partial r}(r^2 C_i U) = \frac{1}{r^2}\frac{\partial}{\partial r}\left(r^2 D_i \frac{\partial C_i}{\partial r}\right) + R_i + R_s \frac{\sqrt{1+a^2}}{a} \qquad (2)$$

where i = species

1 = O_2 ■

2 = CO_2

3 = CO

4 = SO_2

There are four species equations; that is, one for each species. The boundary conditions are the known bulk stream temperature and species compositions at the outer edge of the boundary layer. At the center of the particle the temperature and concentration gradients are zero. Also radiant energy is lost at the particle surface.

4.3 NUMERICAL NODAL ANALYSIS

The discretization equation for this system for node J is derived from the differential equations using a control volume finite - difference method. The discretization equation developed in this manner expresses the conservation of energy or mass species for the finite control volume, just as the differential equation expressed it for an infinitesimal control volume (72). Figure 8 shows the symbols representation of the finite control volume.

If we integrate the energy differential equation over the control volume, we get:

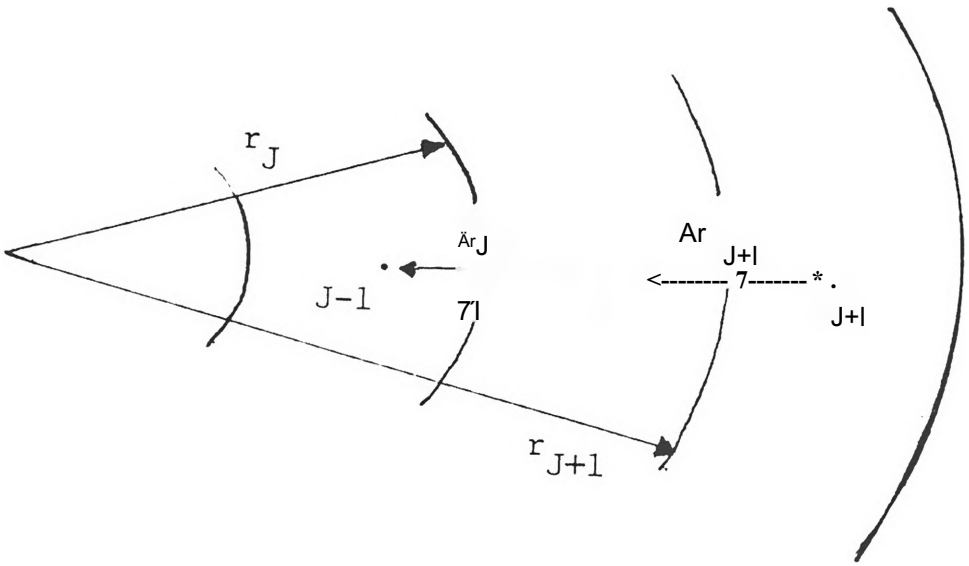

Figure 8. Finite Control Volume

$$\int_{r_J}^{r_{J+1}} [R_h(-\Delta H_h)\, 6r + R_s(-\Delta H_s)\, 2\, 6r \frac{\sqrt{1+\alpha^2}}{a}]\, dr$$

$$= \int_{r_J}^{r_{J+1}} \frac{d}{dr}\left(k r^2 \frac{dT}{dr} + \sum_{i=1}^{4} N_i C_p (T - T^\circ) r^2\right) dr$$

$R_h(-\Delta H_h)\, 0\, (r_{J+1}^3 - r_J^3)/3 + 4H_s)\, e\; a\, R_s\, (r_{J+1}\; r_J$ $\sqrt{1+\alpha^2}$ $\;2 - \;2)$

$$= [-k r^2 \frac{\partial T}{dr} + \sum_{i=1}^{4} N_i C_p (T - T^\circ)\, r^2]_{r_{J+1}}$$

$$- [-k r^2 \frac{\partial T}{\partial r}\Big|_{r_J} + \sum_{i=1}^{4} N_i C_p (T_J - T^\circ)\, r_J^2]$$

Note: $\frac{\partial T}{\partial r}\Big|_{r_{J+1}} = \frac{(T_{J+1} - T_J)}{\Delta r_{J+1}}$

$\frac{\partial T}{\partial r}\Big|_{r_J} = \frac{(T_J - T_{J-1})}{\Delta r_J}$

It is useful to write the energy discretization equation into the following form:

$$a_J T_J = a_{J+1} T_{J+1} + b_{J-1} T_{J-1} + c_J$$

$a_{J+1} = \frac{k\, r_{J+1}^2}{\Delta r_{J+1}} -$ [illegible] $\sum$ [illegible] $(N_i$ [illegible]$)\, r_{J+1}^2$

$$a_{J-1} = k \frac{r_J^2}{\Delta r_J}$$

$a_J = k \frac{r_{J+1}^2}{\Delta r_{J+1}} + \frac{k\, r_J^2}{\Delta r_J}$ [illegible] $\sum$ [illegible] $)$ [illegible]

$$b = \text{^(.днре}^{r^3_{J+1} - r_J^3} + \sqrt{1+\alpha^2} \; <^{\wedge}_{J+1} - <)$$

If we integrate the species differential equation over the control volume, we get:

$$\int_{r_J}^{r_{j+i}} [R_{h_i} r^2 + R_{s_i} \cdot 2 \frac{\sqrt{1+\alpha^2}}{\alpha} r] \, dr$$

$$= \int_J^{J+1} \frac{a}{\partial r} \left(-r^2 D_i \frac{\partial C_i}{\partial r} + r C_i U\right) dr$$

$$R_{h_i} (r_{J+1}^3 - r_J^3)/3 + R_{s_i} \frac{\sqrt{1+\alpha^2}}{\alpha} (r_{J+1}^2 + r_J^2)$$

$$= - r^2_{J+1} \left(D_i \frac{\partial C_i}{\partial r}\right)_{J+1} + r_J^2 \left(D_i \frac{\partial C_i}{\partial r}\right)_J + \left(C_i \bar{U} r^2\right)_{J+1} - \left(C_i \bar{u} r^2\right)_J$$

Note : $\left.\frac{\partial C_i}{\partial r}\right|_J = \frac{(C_{i_J} - C_{h-i})}{\Delta r_J}$

$$\left.\frac{\partial C_i}{\partial r}\right|_{J+1} = \frac{(C_{i_{J+1}} - C_{i_J})}{\Delta r_{j+1}}$$

$$\left.C_i\right|_J = \frac{C_{i_{J-1}} + C_{i_J}}{2}$$

$$\left.C_i\right|_{J+1} = \frac{C_{i_{J+1}} + C_{i_J}}{2}$$

It is useful to write the species discretization equation into the following form:

$$a_{i,J} C_{i,J} = a_{i,J+1} C_{i,J+1} + a_{i,J-1} C_{i,J-1} + b_{i,J-1} r$$

$$a_{i,J+1} = \mathcal{D}_{i_{J+1}} \frac{r_{J-Fl}^{2}}{r_{J+1}}$$

$$a_{i,J-1} = V_{r_J} \wedge + \ddot{u}_J \; r_J^2$$

$$a_{i,J} = \mathcal{D}_{i_{J+1}} \; Ar_{J\cdot"\pm}^{2} \wedge + P \wedge \text{-} \ddot{u} r^2 \; {}_{i^+}Ar_{J+1} \; J+1$$

$$b_i = R_h \left(\frac{r_{J+1}^3 - r_J^3}{3}\right) + R_s \frac{\sqrt{1+\alpha^2}}{\alpha} (r^2_{J+1} - r^2_J)$$

With a 50 node system there will be 50 energy discretization equations and 50 species discretization equations for each of the four species for a total of 250 equations and 250 unknowns.

4.4 MODEL PARAMETERS

The char data, physical data and bulk stream parameters used in the model calculations are given in Table 9.

The reaction rate expressions used are shown on Table 10. Undoubtedly, the kinetics and mechanisms are more complex than assumed; however, similar assumptions have been used by others (73). The sulfur release reaction kinetics are assumed to be proportional to Reaction 2 and 3 shown in Table 9. The proportionality constants a and ß are the moles of ferrous sulfide per mole of carbon and moles of organic sulfur per mole of carbon respectively. The sulfur capture reaction kinetics are taken from the literature as shown on Table 9. Since carbonyl sulfide capture kinetics is first order with respect to the sulfur species

TABLE 9. CHAR DATA, PHYSICAL DATA, AND BULK STREAM PARAMETERS

POROSITY	-	0.35
BET AREA	=	2.1 x 10 m /Kg
DENSITY	=	900 Kg/n/
ASH CONTENT	=	0.5 wt ! ract ion
EMISSIVITY	=	0.9
AVERAGE HEAT CAPACITY OF GAS	»	39.7 7 (KJ/Kg - mol °K)
THERMAL CONDUCTIVITY OF CHAR	=	0.157 (J/m su-ч °K)
THERMAL CONDUCTIVITY OF GAS	=	2 . b 2 7 x 10 x T ' (J/m · sec · K)
DIFFUSIVITY OF 0.,, CO IN GAS FILM =		5. 123 x 10 x T (m /sec)
DIFFUSIVITY OF CO, IN GAS FILM	=	^.211 x 10 x T1' v m ~/s c c)
DIFFUSIVITY OF SO, IN GAS FILM	=	3.538 x 10 x ƒ'J l:n'/secj
KNUDSON DIFFUSION IN CHAR PORES	=	9 700 r — (m /sec)

r : PORE RADIUS IN cm T: °K M: Mole wt of gas
P

SUPERFICIAL GAS VELOCITY = 2 m/sec

PRESSURE = 1 atm

GAS VISCOSITY (KINEMATIC) = 1 3 8. b x 10 m /see

PRANDTL NUMBER = 0.704

$$Nu = 2.0 + .6\,Re^{1/2}\,Pr^{1/3}$$

$$Re = \frac{\text{(Gas velocity)(Particle diameter)}}{\text{(Gas Viscosity)}}$$

TABLE 10. REACTION AND RATE EQUATIONS

REACTION	RATE
$CO + 1/2\ O_2 - CO_2$ Exothermic (Houard et al. (74))	$R_1 - k_1 \exp(-\frac{15,058}{T})\ C_{CO}\ C_{O_2}^{1/2}$ K-mol co/m3 · sec $k_1 = 3.10 \times 10^{?}$ [illegible] $\frac{m^{3/2}}{K\ mol\ sec}$ $-\Delta H\ (298) - 5.65 \times 10^8$ J/K mol O_2
$C + 1/2\ O_2 - CO$ Exothermic (Smith & Tyler (75))	$R_2 = k_2\ T \exp(-$ [illegible]$)\ C_{O_2}$ K-mol C/m2 · sec $k_2 = 3.76$ $(\frac{m}{K\ sec})$ $-\Delta H\ (298) - 2.21 \times 10^8$ J/k mol O_2
$C + CO_2 - 2CO$ Endothermic (Dutta et al. (76))	$R_3 = k_3 \exp(-\frac{29,790}{T})\ C_{CO_2}$ K-mol c/m2 · sec $k_3 - 1.47 \times 10^5\ (\frac{m}{sec})$ $-\Delta H\ (298) - -1.725 \times 10^8$ J/k mol CO_2
$FeS + 3/2\ O_2 - FeO + SO_2$	$R_4 - \alpha R_2$
$(Organic)S + O_2 - SO_2 + CO$	$R_5 - SR_2$
$(Organic)S + CO_2 - COS + CO$	$R_6 = SR_3$
$SO_2 + CaO + 1/2\ O_2 + CaSO_4$ (Wen et al. (77))	$R_7 - k_7 \exp(-$ [illegible]$)\ C_{SO_2}$ K-mol SO_2/m^2 · sec $k_7 = 2.386$ m/sec
$H_2S + CaO - CaS + H_2O$ (Westmoreland et al. (78))	$R_8 = k_8 \exp(-\frac{2597}{T})\ C_{H_2S}$ K-mol H_2S/m^2 · sec $k_8 = 3.732 \times 10^{-4}$ (m/sec)
$COS + CaO - CaS + CO_2$ (Yang et al. (79))	$R_9 = R_8$

and the rate constants is very close to that for H_2S capture, it was assumed that the sulfur capture kinetics of Reaction 8 and 9 are the same. The concentration of COS and H^S are lumped together. Since the development of the mathematical model is independent of the reaction rate expressions used, those parameters and expressions could be easily changed in the model.

4.5 COMPUTER PROGRAM

A FORTRAN program was written to solve the equations derived above. The sequence of computer operations used in this program is shown in Figure 9. Each of the five differential equations are solved by using a tridiagonal matrix algorithm for the finite number of discretization equations written to represent each of the five differential equations. Since, the coefficients of the discretization equations are dependent on the solution of the other four differential equations, an iterative method is used until all five of the differential equation solutions agree. A copy of the FORTRAN program used for this model is given in Appendix C.

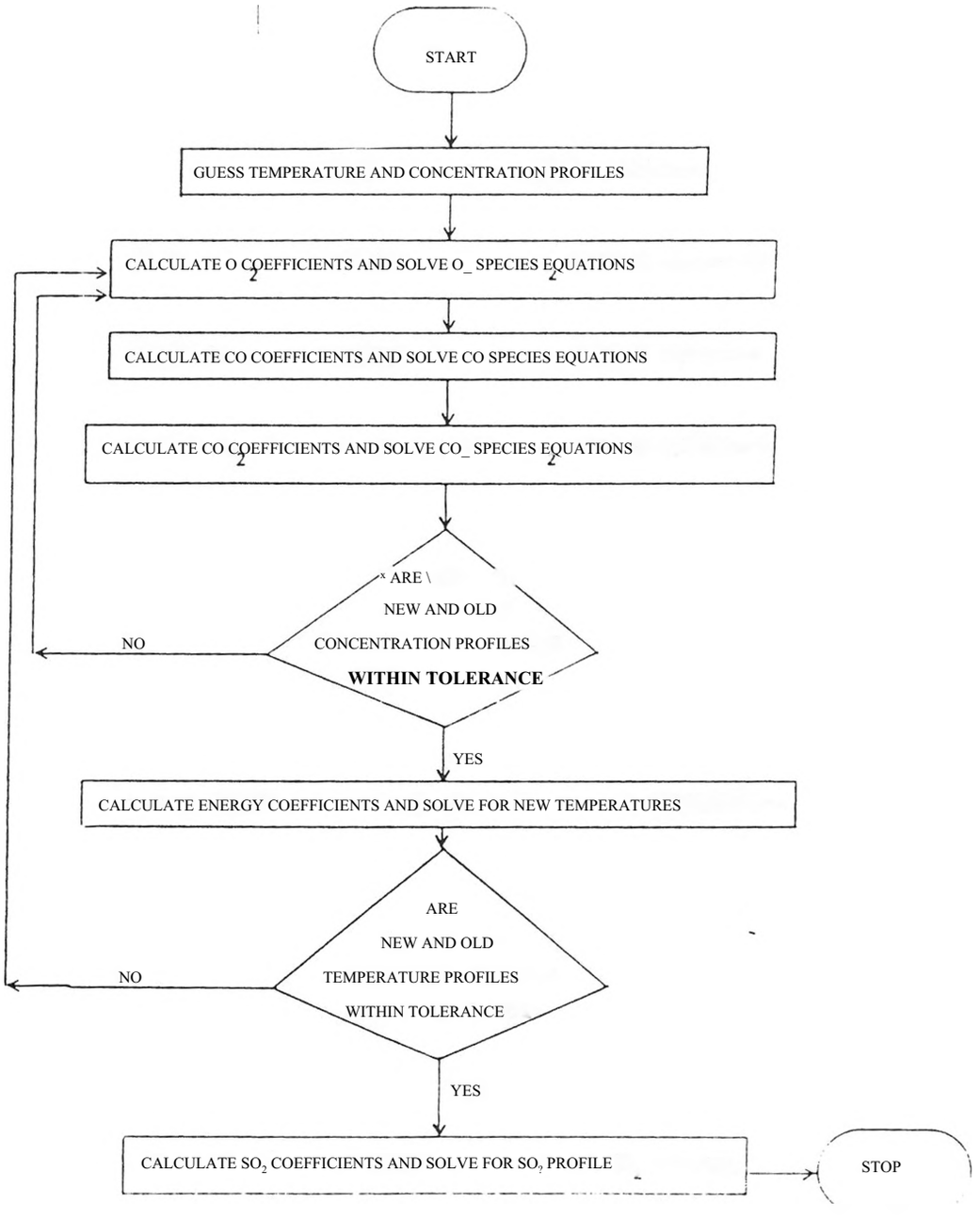

Figure 9. Computer Program Outline

V. MODEL RESULTS

5.1 IGNITED AND UNIGNITED PARTICLE STATES

The model results reveal that lignite char particles can exist in a fluidized bed combustor either in an ignited state or an unignited state depending on particle radius, bed temperature and oxygen concentration. Figure 10 shows particle temperature versus bed temperature for a 1mm diameter particle with the bulk stream *02'^2'* and CO at 13, 3.6, and 7.2 mole percent respectively.

It should be noted that the particle temperature is only slightly higher than the bed temperature for bed temperatures below 1100 degrees Kelvin. When the bed and particle temperatures are only slightly different the particle is considered unignited. Actually, the gas film reactions are unignited with heterogeneous reactions occurring in the particle pores. This is a result of the diffusion process being fast relative to the reaction rate of carbon monoxide with oxygen. The carbon monoxide escapes to the bulk with very little reaction occurring.

At bed temperatures greater than 1120 degrees Kelvin, the particle temperature is much greater than the bed

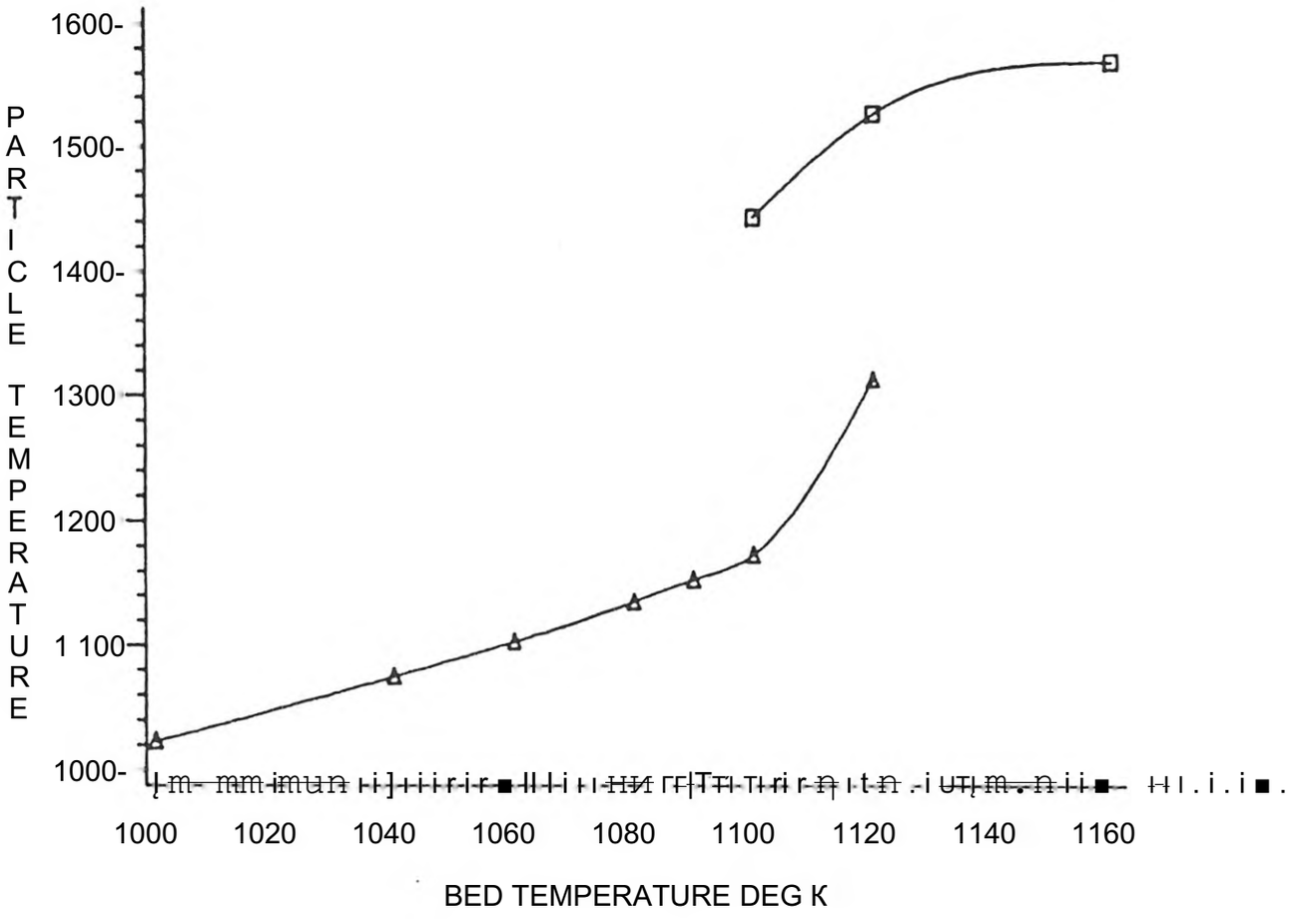

Figure 10. Particle Temperature vs. Bed Temperature, 0^ = 13%, r^ = . 5 mm

temperature. This is a result of heat being generated by carbon monoxide burning in the gas film. When this condition exists the particle is considered ignited.

Multiple solutions to the model differential equations exist between the ignited and unignited states. This transition zone occurs at higher bed temperatures for smaller particles. By decreasing the particle radius the diffusion process in the gas film becomes very fast relative to the carbon monoxide reaction process. If char combustion is performed in humid air the transition zone occurs at lower bed temperatures compared to combustion in dry air. This is a result of the water acting as a catalyst in the carbon monoxide reaction with oxygen. Other workers have shown that particles undergo ignition for initial bed temperatures higher than a critical value and extinction after some conversion level (73).

Figure 11 shows the concentration profiles for an unignited particle. This figure shows that our definition of an unignited particle actually means a particle that is unignited in the boundary layer. The $O_{2\ r}$ CO_2 and CO profiles are relatively flat in the boundary layer, but strong concentration gradients exist in the particle. This indicates the combustion reactions are occurring within the particle. The SO_2 concentration peaks at the particle

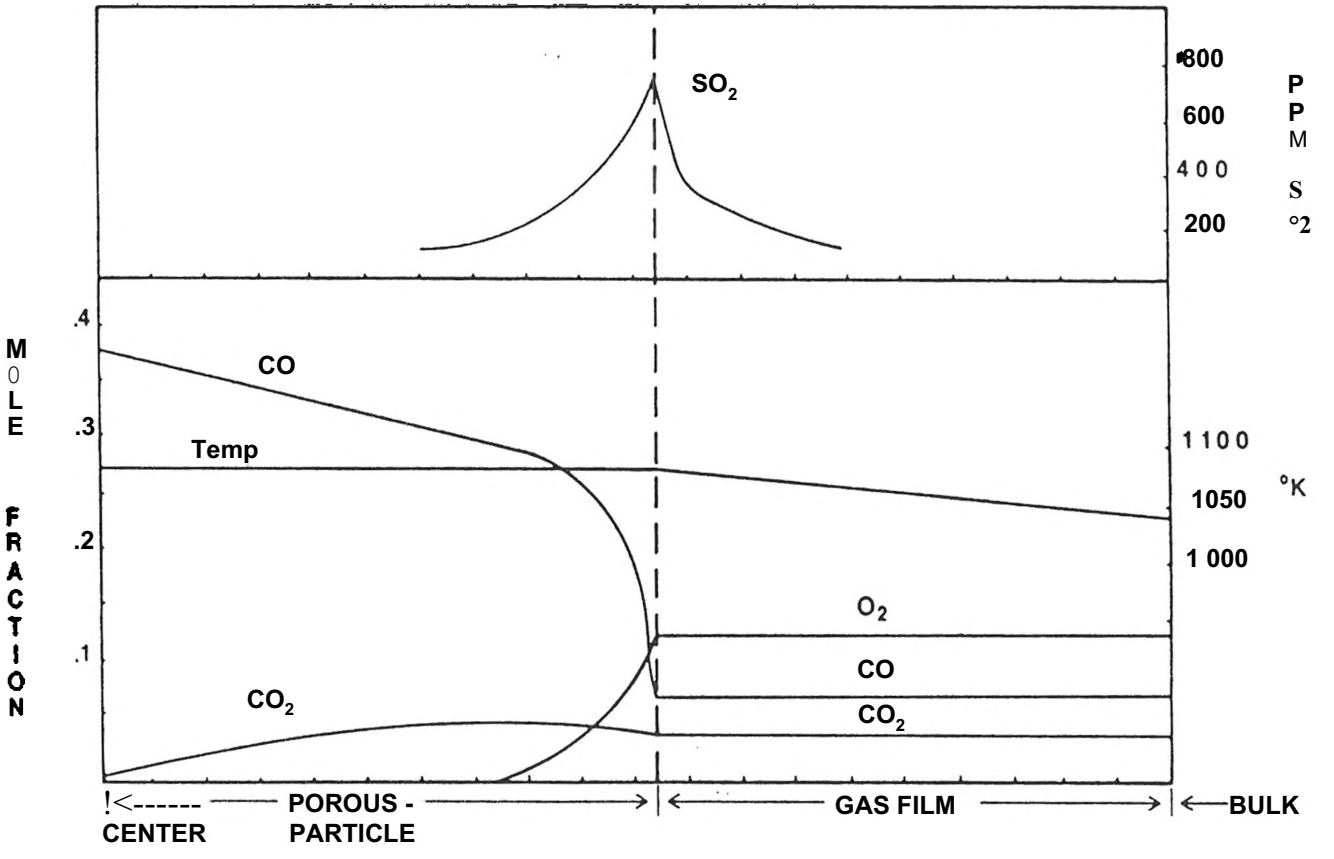

Figure 11. Unignited Particle Concentration and Temperature Profile

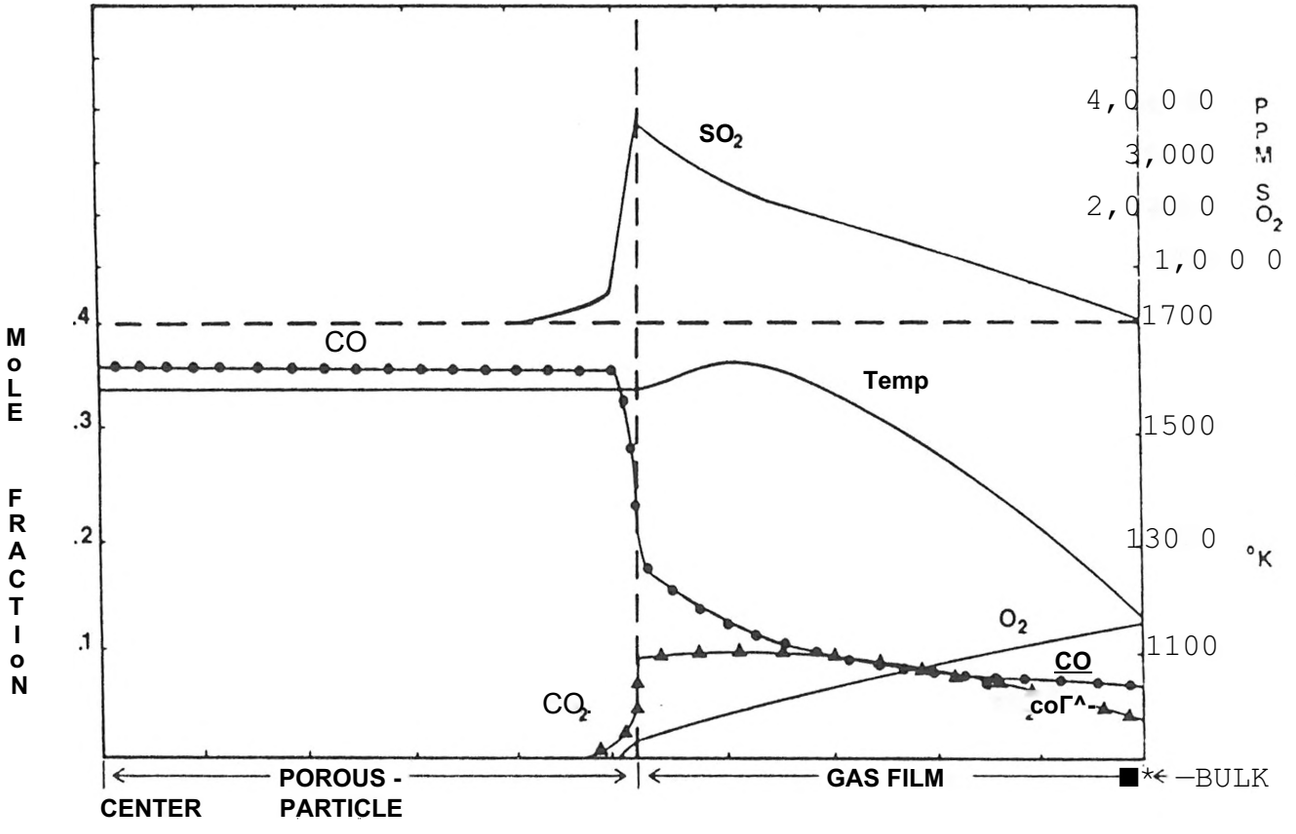

Figure 12. Ignited Particle Concentration and Temperature Profile

surface at about 700 parts per million.

Figure 12 shows the concentration profile for an ignited particle. This figure indicates combustion of CO occurring in the gas film. Both the CO_2 concentrations and the temperature peak in the gas film surrounding the particle. The SO_2 profile peaks at the surface at about 3800 parts per million. This is a much higher SO_2 concentration than that calculated for the unignited particle.

5.2 EFFECT OF BED TEMPERATURE ON SULFUR CAPTURE

Figure 13 shows the fraction of sulfur capture versus bed temperature for the same particle size and conditions as in figure 10. A decrease in fraction of sulfur capture as bed temperature increases is shown for the unignited particle state. This can be explained by the fact that in the unignited state the particle combustion is reaction rate controlled and the sulfur release rate increases more with temperature than does the capture rate due to its higher activation energy.

A slight increase in the fraction of sulfur capture as bed temperature increases is shown for the ignited particle state. This can be explained by the fact that in the ignited state the particle combustion is becoming more

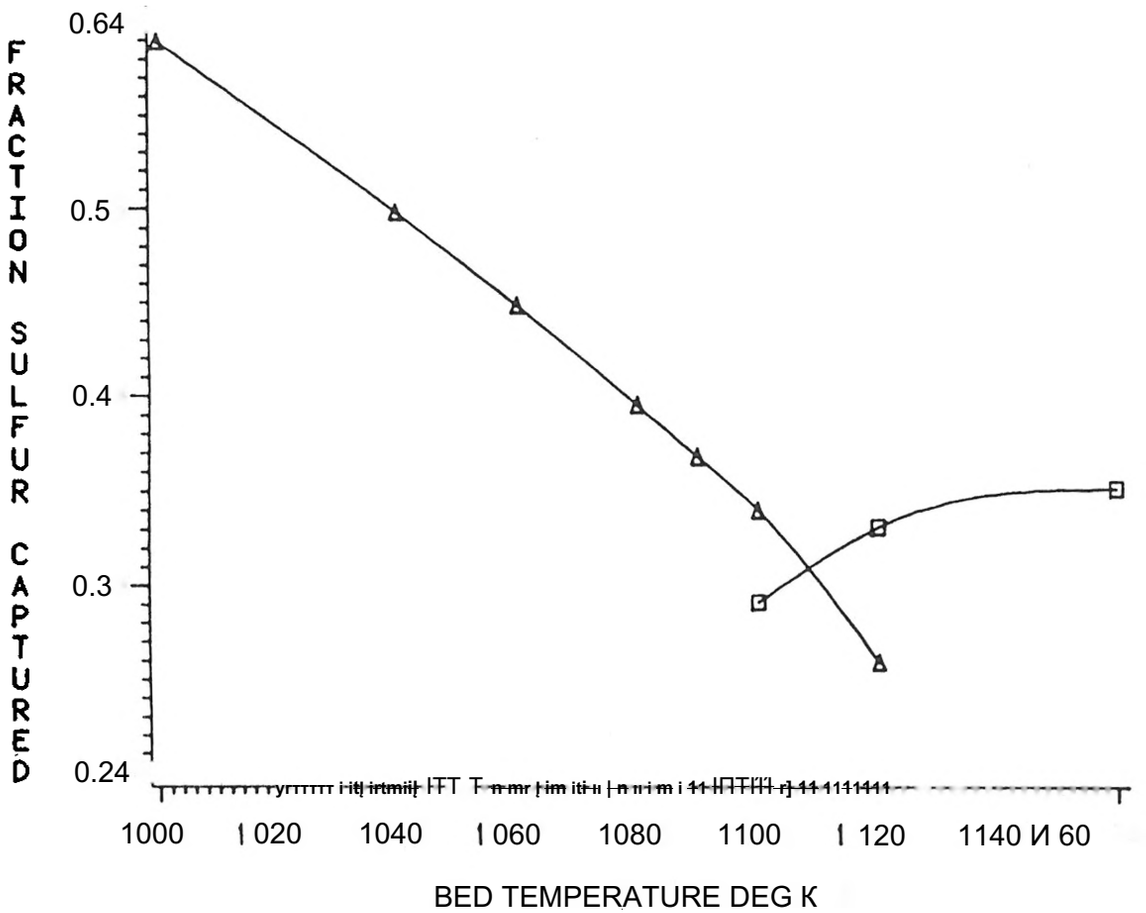

Figure 13. Sulfur Capture vs. Bed Temperature, 0^ = 13%, r^ = .5 mm

diffusion controlled. That is the rate of oxygen depletion and sulfur dioxide generation is fast compared to the rate of diffusion of these species across the gas film. The higher the particle temperature becomes the more the particle combustion and sulfur release becomes diffusion controlled. Since the sulfur release rate becomes fast compared to the rate of diffusion of sulfur dioxide away from the particle, the sulfur capture rate increases due to an increase of sulfur dioxide concentration in the pores as well as to the effect of temperature on the reaction rate constant.

5.3 EFFECT OF OXYGEN COMPOSITION ON SULFUR CAPTURE

Figure 14 shows the fraction of sulfur capture versus oxygen composition for a 3mm particle at a bed temperature of 1000 dgrees Kelvin. In the unignited particle state, sulfur capture is calculated to be almost independent of oxygen bulk stream composition. This is due to the fact that changes in oxygen composition has very little effect on the particle temperature for particles in the unignited state. For a change of oxygen composition from .1 to . 12, for the particle in figure 14, the particle temperature went up only 3 degrees Kelvin. Due to the increse in oxygen the sulfur release rate went up slowly, but so did

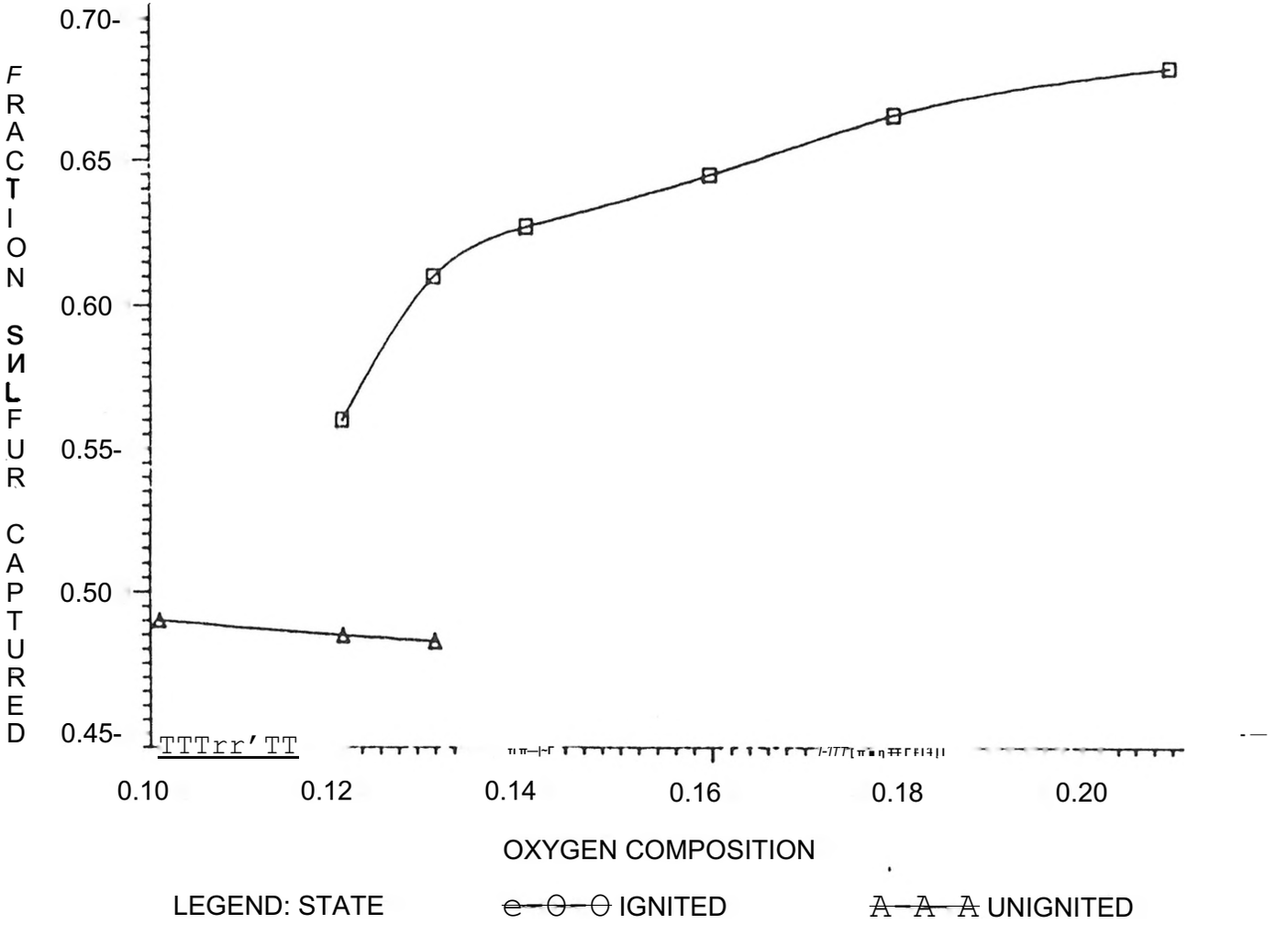

Figure 14. Sulfur Capture vs. Oxygen Composition, = T$_b$000°K, r = 1.5 mm$_c$

the capture rate due to an increase in SO2 concentration. The net result is very little change in sulfur capture.

In the ignited particle state sulfur capture increases with the oxygen bulk stream composition. This happens because the particle combustion becomes more diffusion controlled as you increase oxygen composition. As the oxygen composition is increased in the gas film the carbon monoxide burns faster. This produces higher particle temperatures and results in lower oxygen compositions in the pores. The sulfur capture rate actually increases due to higher particle temperatures and higher sulfur dioxide concentrations in the pores.

Figure 15 shows the fraction of sulfur capture versus oxygen composition for a 1mm particle at a bed temperature of 1000 degrees Kelvin. We observe the same trends for the particle in both the ignited and unignited particle state that we observed for the larger particle in figure 14. However, we see a drop in the sulfur capture as we go from the unignited state to the ignited state. In the larger particle case, we observe an increase in the sulfur capture as we go from the unignited to the ignited particle state. This will be explained in the next section.

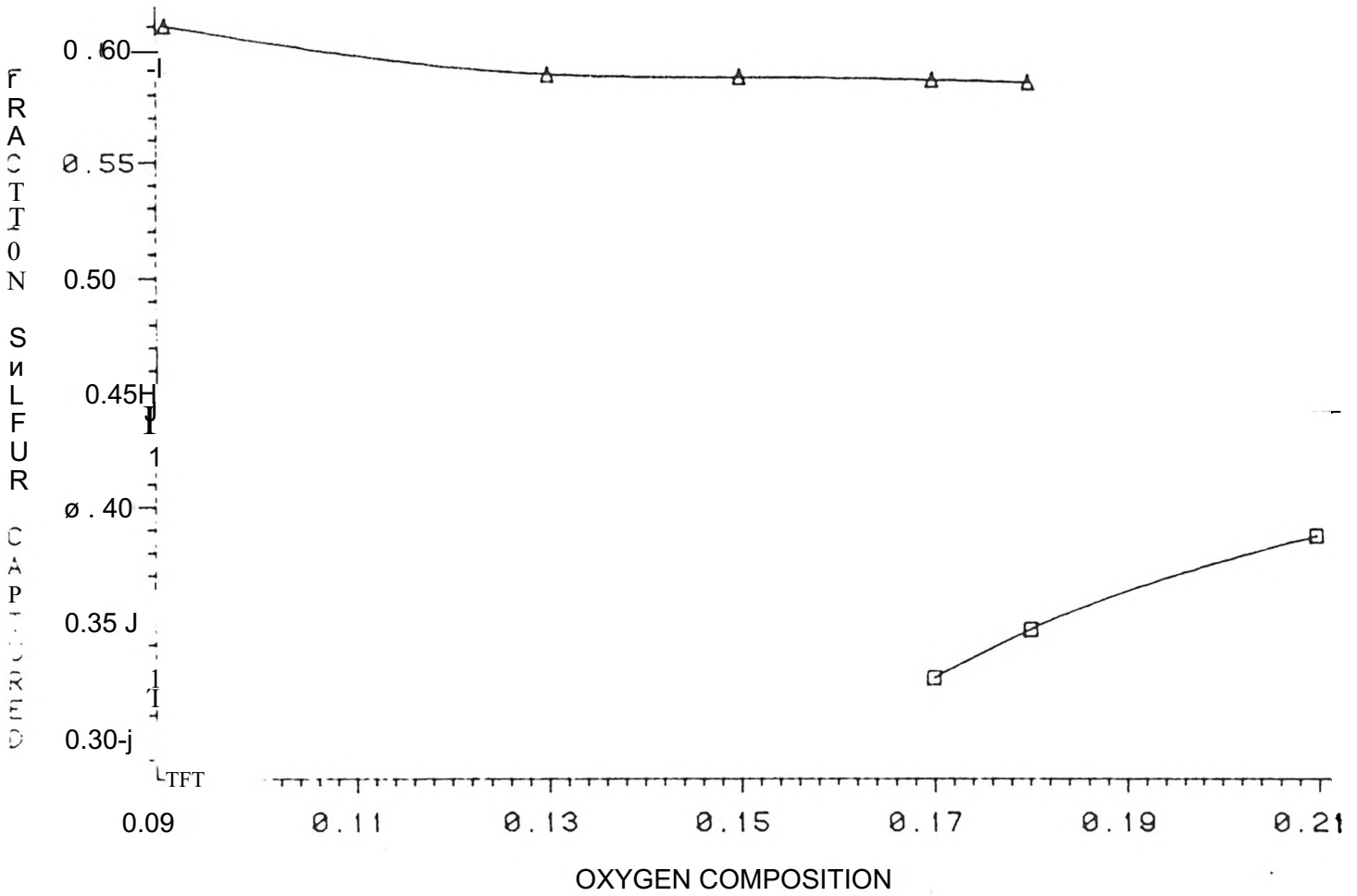

Figure 15. Sulfur Capture vs. Oxygen Composition, T_b = 1000°K, r_c = .5 mm

5.4 EFFECT OF PARTICLE SIZE ON SULFUR CAPTURE

Figure 16 shows the effect of particle size on sulfur capture for particles in the ignited state. This plot is for a bulk stream temperature of 1000 degrees Kelvin, oxygen composition of 18 percent, carbon monoxide composition of 2.8 percent, and carbon dioxide composition of 1.4 percent.

Sulfur capture increases with particle radius for particles in the ignited state. This can be explained by the fact that the larger particles have a larger gas film thickness. This makes the particle combustion more diffusion controlled. We have discussed previously how the capture of sulfur increases as the combustion becomes more diffusion controlled for ignited particles. Figure 17 shows the particle temperatures for particles of the same size and bulk stream conditions of those shown in figure 16. The particle temperature of ignited particles increase with decrease in particle size.

In the unignited state the sulfur capture decreases with increase in particle size. The sulfur capture for the 3mm diameter particle in the unignited state at 13 percent oxygen composition is approximately 49 percent as shown in figure 14. The sulfur capture for the 1mm diameter particle in the unignited state at 13 percent oxygen

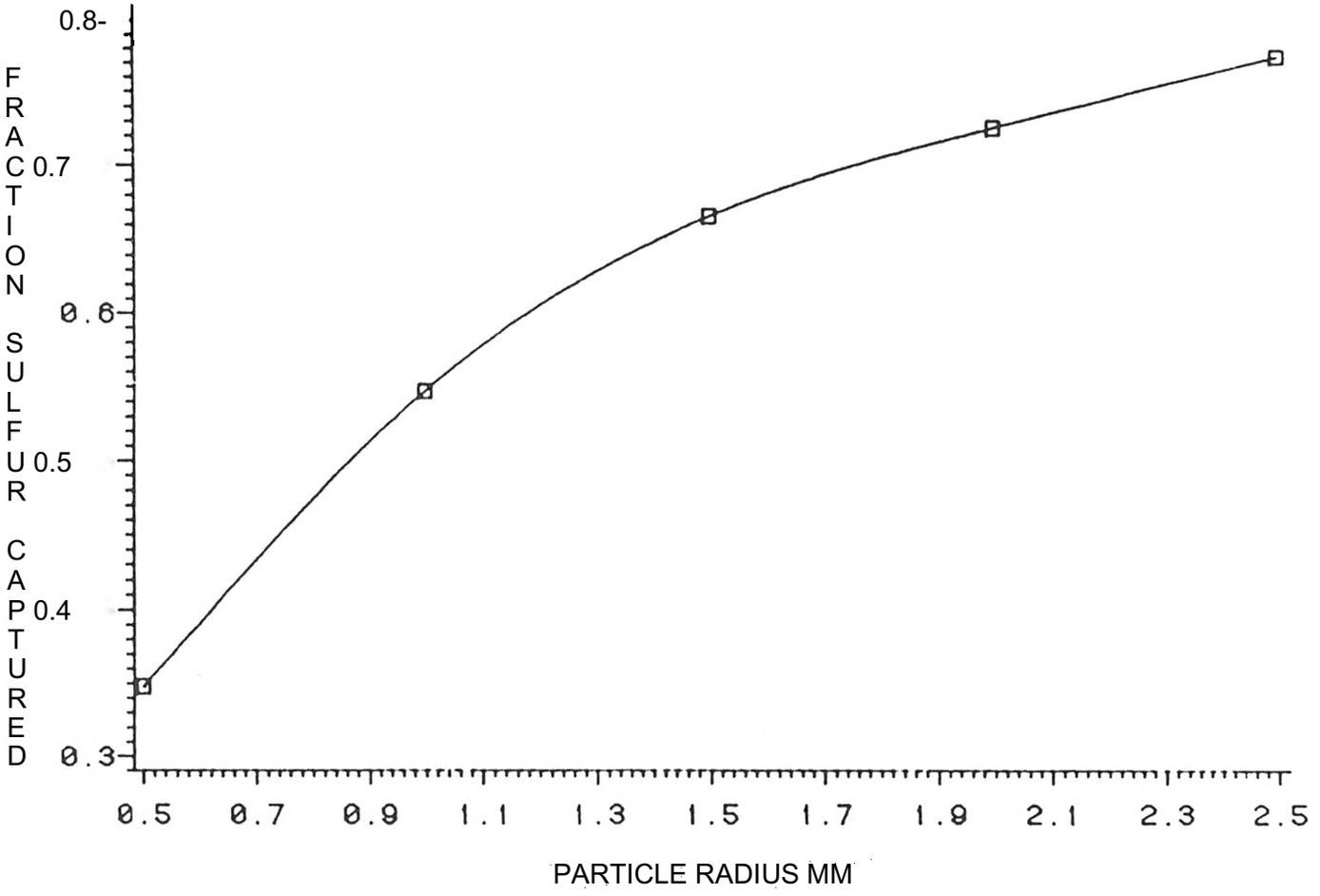

Figure 16. Sulfur Capture vs. Particle Size, O,, = 18%, T_{t} = 1000°K

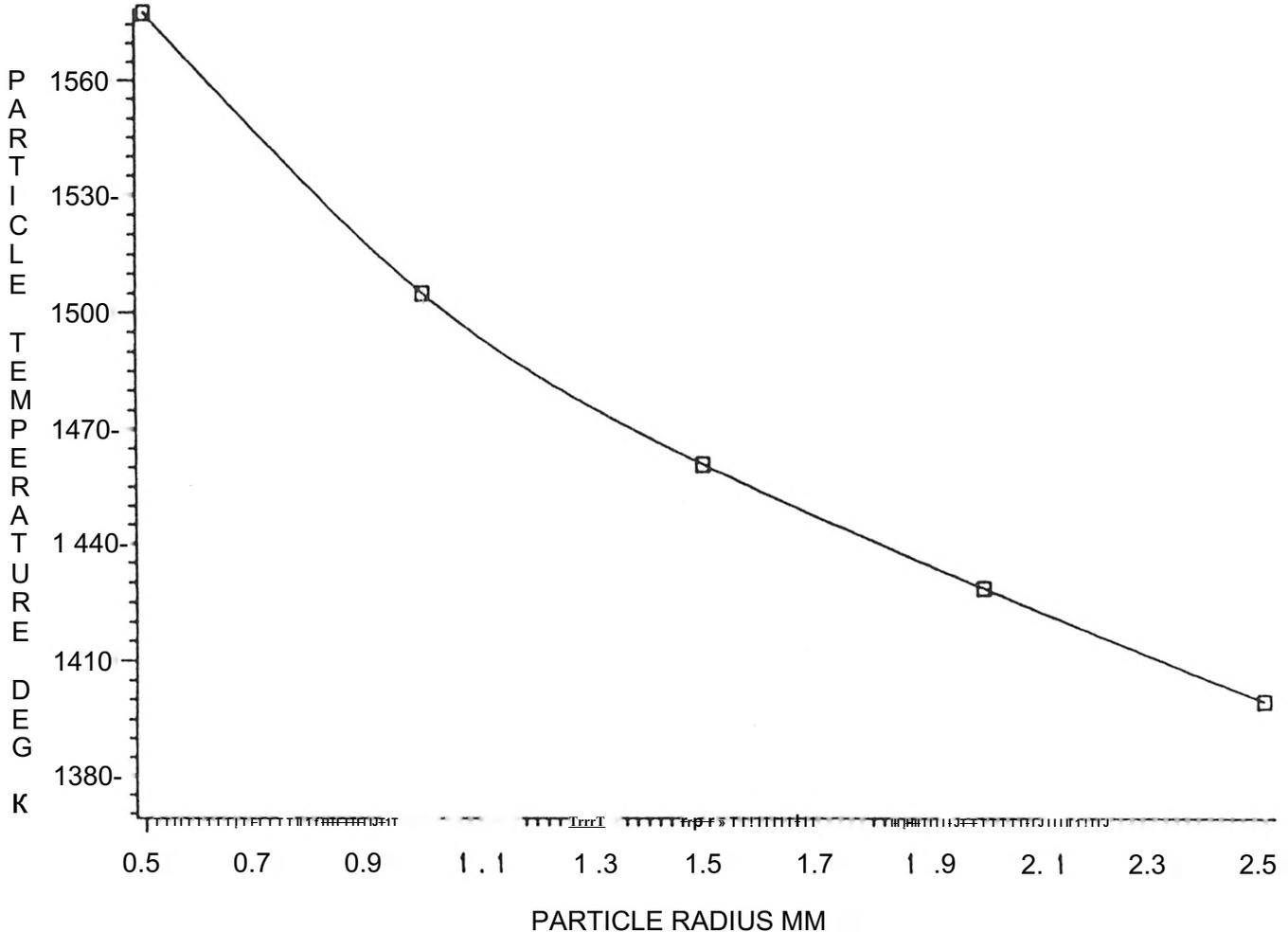

Figure 17. Particle Temperature vs. Particle Size, = 18% O_2 T_D = 1000°K

composition is approximately 58 percent as shown in figure 15. The particle combustion of the unignited particles are reaction rate controlled. Since, the larger particles provide more surface area for the char combustion, the particle temperatures are higher for the steady-state solution of larger particles. As we mentioned earlier the sulfur release rate increases more with temperature than does the capture rate due to its higher activation energy.

5.5 EFFECT OF CO_2 AND CO ON SULFUR CAPTURE

The model revealed that the carbon dioxide concentration in the bulk stream had negligible effect on the sulfur capture for particles in the unignited state. However, increasing carbon monoxide in the bulk stream actually decreases capture. By increasing the carbon monoxide the particle temperature is increased and the sulfur capture decreases. The reaction of carbon monoxide with oxygen is first order with respect to carbon monoxide and one-half order with respect to oxygen. So increasing carbon monoxide concentration has a greater effect on particle temperature than does increasing oxygen. As mentioned earlier the sulfur release rate increases more with temperature than does the capture rate for unignited particles.

The sulfur capture of ignited particles can be increased by increasing the carbon monoxide concentration in the bulk stream. By increasing the carbon monoxide concentration, the reaction rate of oxygen with carbon monoxide increases in the gas film causing the particle temperature to climb. This results in the particle combustion becoming more diffusion controlled. Therefore , sulfur capture increases. Increasing carbon dioxide in the bulk stream tends to reduce the particle temperature for ignited particles. However, the change in temperature is not great enough to affect the sulfur capture.

VI. COMPARISON OF EXPERIMENTAL MEASUREMENTS AND MODEL RESULTS

Since the char model calculates the amount of sulfur retained by the ash after devolatilization, the sulfur that leaves the particle with the volatiles is an adjustable parameter. Figure 18 shows the experimental data and char model results for sulfur capture versus bed temperature at an oxygen composition of 13%. This figure shows that from 1000°K to about 1140°K the trends are the same for both the experimental data and the computer results. For this graph it was assumed that 45% of the original coal sulfur was released during devolatilization. Actually by choosing a lower devolatilization sulfur release fraction the model results would agree with the experimental data from 1000°K to 1140°K.

As the bed temperature is decreased below 1000 degrees Kelvin the char model sulfur capture continues to increase while the experimental data decreases. This is a result of the assumption used in the model that all of the $CaCO_3$ had changed to CaO during devolatilization. This assumption is not valid below 1000°Kelvin. At temperatures below a 1000° Kelvin the conversion of $CaCO_3$ to CaO is not complete. Since less CaO is available for sulfur capture as you decrease

the temperature, you expect a decrease in sulfur capture with a decrease in bed temperature as was measured experimentally .

Figure 19 shows the experimental data and char model results for sulfur capture versus oxygen composition. The trends are the same for both the experimental data and the char model results. The experimental data shows that there is very little change in sulfur capture at the low oxygen compositions. The model suggests that this is a result of the particles being in the unignited state. At an oxygen composition of about .09 the sulfur capture increases quickly and then plateaus. The model suggest that the particles are becoming ignited. As the oxygen is increased the particle temperatures will increase and the combustion reactions become more diffusion controlled. This results in the sulfur capture increasing with oxygen quickly at first and then leveling off as the system becomes diffusion controlled.

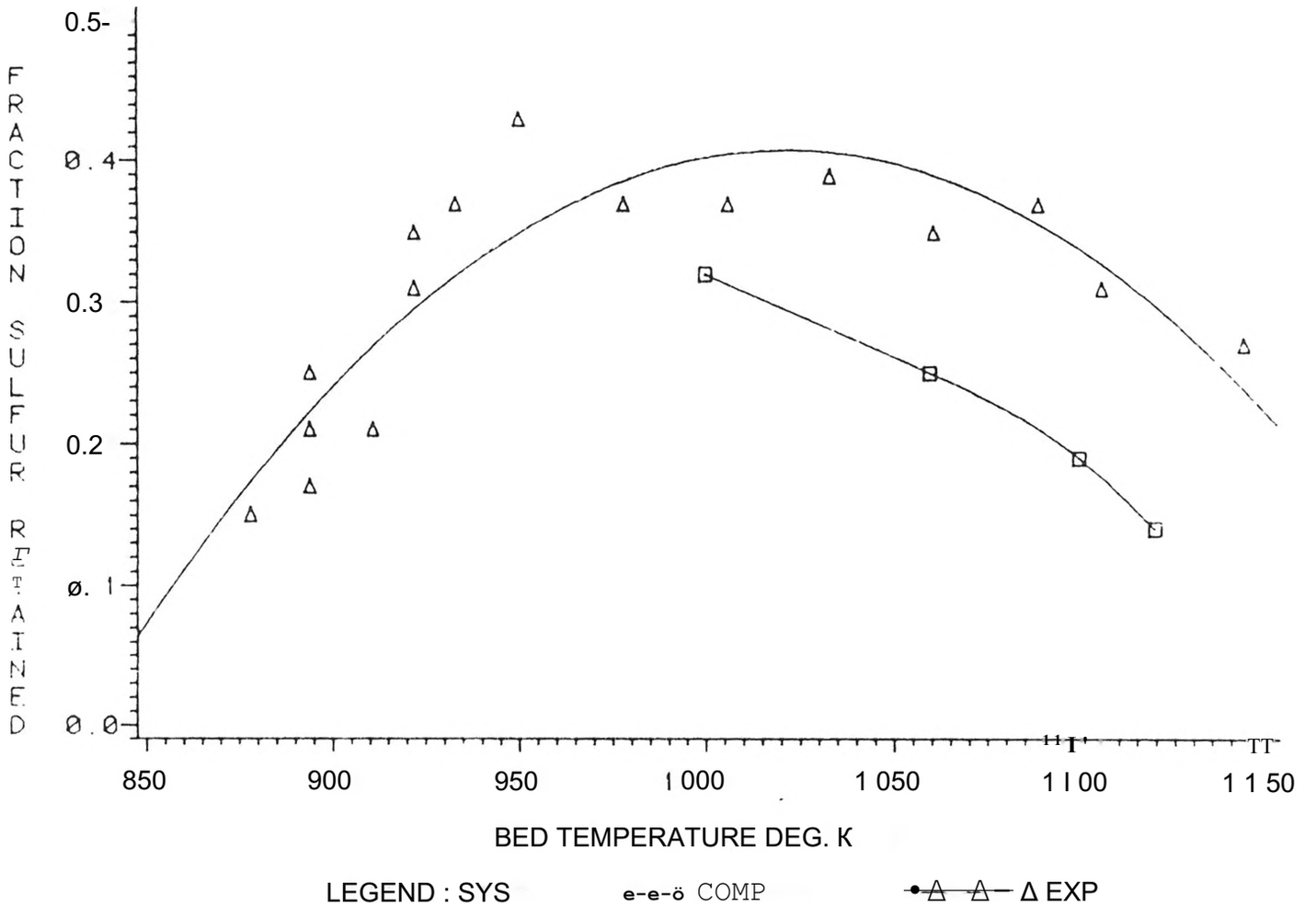

Figure 18. Sulfur Capture vs. Bed Temperature

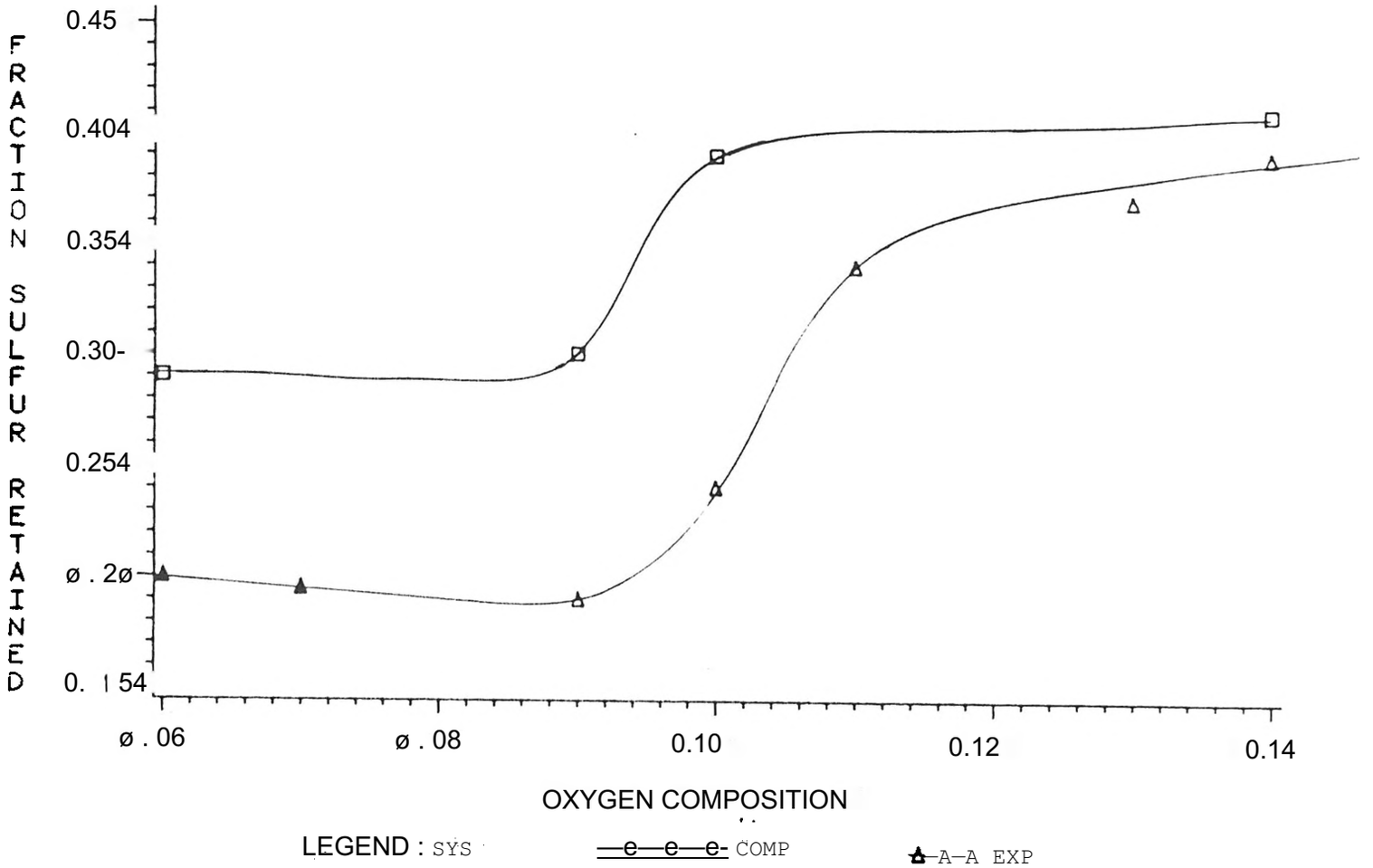

Figure 19. Sulfur Capture vs. Oxygen Composition

NOMENCLATURE

a_1 ƒ Coefficient in the Species Nodal Equation, L/t^3

a_J Coefficient in the Energy Nodal Equation, Q/tT

b, b^ Parameter in the Energy and Species Nodal Equation, Q/t, M/T

C^ Concentration of gas species i, M/L^3

$\bar{C}_{PT}$ Mean heat capacity, Q/MT

D_i Diffusivity of gas species i, L^2/t

H^ Heat of reaction for homogeneous reactions, Q/M

H_g Heat of reaction for heterogeneous reactions, Q/M

J Nodal index, dimensionless

k Thermal conductivity, Q/LtT

K Reaction rate constant

N^ Molar flux of species i, M/L^2t

Nu_P Particle Nusselt Number, dimensionless

Pr Prandi Number, dimensionless

r Radial position, L

r_r Radial position to outer edge of the boundary layer , L

r_U Radial position to the Jth Nodal position, L

Гp Pore radius, L

r_c Char particle radius, L

Ar_3 Nodal radial finite difference, L

R_h	Homogeneous reaction rates, M/L^3t
R_s	Heterogeneous reaction rates, M/L^2t
Re	Reynolds Number, dimensionless
T	Temperature, T
T_R°	Reference temperature, T
U	Convective velocity in the boundary layer, L/t

Greek Letters

α	r_p/r_c , dimensionless
e	porosity, dimensionless

BIBLIOGRAPHY

1. Speight, J.G., The Chemistry and Technology of Coal, Marcel Dekker Inc., New York, 1983.

2. Probstein, R.F., Synthetic Fuels, McGraw-Hill, New York, 1982.

3. Meyers, R.A., Coal Structure, Academic Press, New York, 1982 .

4. Attar, A., "Chemistry, Thermodynamics and Kinetics of Reactions of Sulfur in Coal-Gas Reactions: A Review," Fuel, 52, 1978.

5. Deubrouck, A.W., "Sulfur Reduction Potential of the Coals of the United State," U.S. Bureau of Mines, Washington, D.C., 1972.

6. Cox, J.T., "Coal Weathering: Causes, Effects and Implications," ACS Division of Fuel Chemistry Preprints, No. 1, 29, 1984.

7. Gladfelter, W.L., Dickerhoof, D.W., "Determination of Sulphur Forms in Hydrodesulphurized Coal," Fuel, 55, 355 (1976).

8. Stopes, M.C., "System of Lithotypes," Proc. Roy Soc. 8., London, 470 (1919).

9. Renton, J.J., "Semi-Quantitative Determination of Coal Minerals By X-Ray Diffractometry", ACS Division of Fuels Preprints, No. 4, 29, 1984.

10. Montano, P.A. and Bommannavar, A.S., "High Temperature Transformation of Minerals in Coal and the Relationship to Organic Structure," ACS Division of Fuels Preprints, No. 1, 29., 19 84.

11. Thiessen, R., U.S. Bureau of Mines, 564 (1935).

12. ASTM Standards, Part 26D3177 (1981), 380.

13. ASTM Standards, Part 26D2492 (1981), 319.

14. Stewart, I. and Whiteway, S.G., "Decomposition of Pyrite in a Coal Matrix During Pyrolysis of Coal," ACS Division of Fuel Chemistry Preprints, No. 4, 29, 1984.

15. Parr, S.W., "University of Illinois Engineering Experiment Station Bulletin," 180, 1928.

16. Harvey, R.D. and Ruch, R.R., "Overview of Mineral Matter In U.S. Coals," ACS Division of Fuel Chemistry Preprints, No. 4, 29 , 1984.

17. Mackowsky, M., Coal Petrology, Gebrüder Borntraeger, Berlin, 153 (1982).

18. Attar, A., "Chemistry, Thermodynamics and Kinetics of Reactions of Sulphur in Coal-Gas Reactions: A Review", Fuel, 57, 1978.

19. Perry, R.H. and Chiton, C.H., Chemical Engineering Handbook, 5th Edition, McGraw-Hill, 20-64, 1973.

20. Breuer, C.T., "Retrofitting Coal-Fired Boilers Economics For Process Plants," Chemical Engineering, No. 19, 91, 1984 .

21. Fernelly, P.F., C.W. Young, G. Tuckel, and E. Peduto, "1983 Long-Term Emission Monitoring at the Georgetown University Fluidized-Bed Boiler", U.S. DOE Report No. DOE/METC: 83-48.

22. Modrak, T.M., J.T. Tang and C.J. Aulissie, "1982 Sulfur Capture and Nitrogen Oxide Reduction on the 6'x6' Atmosphere Fluidized Bed Combustion Test Facility Electric Power Research Instutite, Palo Alto, CA," Symposium on Combustion Chemistry, American Chemical Society, Las Vegas, NV, 1982.

23. DeJong, J.A.H. and F.F. Nomden, Power Technol., 9:91, (1974).

24. Davidson, J.F. and Harrison, D., Fluidized Particles, Cambridge University Press, 1973.

25. Partridge, B.A. and Rowe, P.N., Trans. Inst. Chern. Eng. London, 4£, T-335 (1966).

26. Szekely, J, Trans. Inst. Chern. Eng. London, 197 (1962).

27. Chiba, T. and Kobayashi, H. , Chern. Eng. Sci., 25 , 1375 (1970) .

28. Davies, L. and Richardson, J.F., Trans. Inst. Chern. Eng. London, 44, T-293 (1966).

29. Pereira, J.R. and Calderbank, P.H., Proc. Fluidized Combustion Conference, Inst. Fuel, London, Paper B.2, Sept. 1975.

30. Kunii, D. and Levenspiel, 0., Fluidization Engineering, Krieger, New York, 1969.

31. Kruse, C.W. and Shimp, N.F., "Removal of Organic Sulfur By Low-Temperature Carbonization of Illinois Coals," J. AIChE, 1981.

32. Moffat, A.J., "The Chemistry and Mechanism of Sulfur Relase During Coal Combustion," Not published.

33. Medvedev, K.P. and Petropolskaya, UKHIN, 19, 137 (1968).

34. Attar, A., Corcoran, A.H., and Gibson, G.S., ACS Division of Fuel Chemistry Preprints, 21, 106 (1976).

35. Schwab, G.M. and Philinis, J.J., "Reactions of Iron Pyrite: Its Thermal Decomposition and Reduction By Hydrogen and Air Oxidation," ACS, 69 , 2588 (1947) .

36. Martin, L.G., Larson, J.W. and Wender, I., Coal Science, Academic Press, New York, Vol. 1, 1982.

37. Wasburn, E.W., Proceedings of National Academy of Science, 7, 115 (1921).

38. Tsai, S.C., Fundamentals of Coal Beneficiation and Utilization, Elsevier Scientific Publishing Company, Amsterdam-Oxford-New York.

39. Phillips, R., Vastóla, F.J. and Walker, P,L., Jr., "Fractors Affecting the Product Ratio of Carbon-Oxygen Reaction, I and II," Carbon, 7, 479 (1969); Carbon, 8, 205 (1970) .

40. Davis, H. and Hottel, H.C., "Combustion Rate of Carbon. Combustion at a Surface Overlaid With Stagnant Gas," Ind. Eng. Chern., 2 6 , 8 8 9 (19 3 4).

41. Wicke, E. and Wurzbacher, G., "Koncentrations Profile ver einer in Saverstoffstrom verbrennenden Kohlenstoffioberflache - I. Experimentelle Ergebnisse," Int. J. of Heat Mass Transfer, 5 , 277 (1962) .

42. Kish, D., "Uber den Temperature Lauf von in Saverstoffstrom brennenden Graphitober Flachen," Ber. Bunsonges. Phys. Chern., 71, 60.

43. Smith, D.F. and Gudmundsen, A., "Mechanism of Combustion of Individual Particles of Solid Fuels", Ind. Eng. Chern., 23, 277 (1931) .

44. Kurylko, L. and Essenhigh, R.H., "Steady and Unsteady Combustion of Carbon," Fourteenth Symposium (International) on Combustion, p. 1375, The Combustion Institute, 1973.

45. Brothers, J.A., "Proceedings of the 1983 International Conference on Coal Science", Pittsburgh, 537 (1983).

46. Stone, R.R., Anthony, R.G., and Bullin, J.A., "Sulfur Removal From Texas Lignite Using Steam and Air," Fuel Processing Technology, 5^, 65 (1981).

47. Lernie, Simil, S., Fuel, 41, 141 (1962).

48. Ranz, W.E. and Marshall, W.R., Jr., "Evaporation From Drops, I and II," Chern. Eng. Prog., 48 , 141 (1952) .

49. Frossling, N., "Uber die Verdunstung fallender Tropfen," Gerlands Beitr. Geophys., 52, 170 (1938).

50. Lewis, W.K., "Chemistry of Combustion In Coal-Fired Furnaces," Ind. Eng. Chem., 15, 502 (1923).

51. Nusselt, W., "Der Verbrennungsvorgang in der Kohlenstaubfeverong," Ver. Deut♦ Ing. , 68 , 124 (1924) .

52. Burke, S.P. and Schumann, T.E.W., "Kinetics of a Type of Heterogeneous Reactions," Ind. Eng. Chern., 23, 406 (1931) .

53. Burke, S.P. and Schumann, T.E.W., "The Mechanism of Combustion of Solid Fuel," Proc. 3rd Int. Conf. Bituminus Coal, 2, 485 (1931)1

54. Spalding, D.B., "Combustion of Fuel Particles," Fuel, 30 , 121 (1951) .

55. van der Held, E.F.M., "The Reaction Between a Surface of Solid Carbon and Oxygen," Chern. Eng. Sci. , 14, 300 (1961) .

56. Khitrin, L.N., Physics of Combustion and Detonation, Moscow University Press, 1957.

57. Hugo, P., Wicke, E. and Wurzhacher, G., "Konzentration-sprofile ver einer in Saverstoffstrom verbrennenden Kohlenstoffoborflache - II. Berechnung der Kunzentrationsprofile," Int. J. Heat Mass Transfer, 5,, 929 (1962) .

58. Caram, H.S. and Amundson, N.R., "Diffusion and Reaction in a Stagnant Boundary Layer About A Carbon Particle," Ind. Eng. Chern. Fund., 16 , 171 (1977) .

59. Mon, E. and Amundson, N.R., "Diffusion and Reaction in A Stagnant Boundary Layer About a Carbon Particle, 2. An Extension," Ind. Eng. Chern., Fund., 17, 313 (1978).

60. Mon, E. and Amundson, N.R., "Diffusion and Reaction in A Stagnant Boundary Layer About a Carbon Particle, 3. Stability,", Ind. Eng. Chern. Fund., 18, 162 (1979).

61. Mon, E. and Amundson, N.R., "Diffusion and Reaction in a Stagnant Boundary Layer About a Carbon Particle, 4. The Dynamical Behavior," Ind. Eng. Chern. Fund., 19, 243 (1980).

62. Sundaresan, S. and Amundson, N.R., "Diffusion and Reaction in a Stagnant Boundary Layer About a Carbon Particle, 5. Pseudesteady State Structure and Parameter Sensitivity," Ind. Eng. Chern., Fund., 19, 344 (1980).

63. Sundaresan, S. and Amundson, N.R., "Diffusion and Reaction in a Stagnant Boundary Layer About a Carbon Particle. 6. Effect of Water Vapor on the Pseudosteady State Structure," Ind. Eng. Chern. Fund., 19, 351 (1980).

64. Sundaresan, S. and Amundson, N.R., "Diffusion and Reaction in a Stagnant Boundary Layer About a Carbon Particle. 7, Transient Behavior and Effect of Water Vapor," AIChE J., 27, 679 (1981).

65. Ubhayakar, S.K. and Williams, F.A., "Burning and Extinction of a Laser-Ignited Carbon Particle in Quiescent Mixtures of Oxygen and Nitrogen," J. Electro-chem. Soc., 123, 747 (1976).

66. Gavalas, G.R., "Analysis of Char Combustion Including the Effect of Pore Enlargement," Comb. Sci. Technoi., 24, 197 (1981).

67. Srinivas, B. and Amundson, N.R., "Intraparticle Effects in Char Combustion. I. Steady-State Analysis," Can. J. Chern. Eng., 58, 476 (1980) .

68. Srinivas, B. and Amundson, N.R., "Intraparticle Effects in Char Combustion, III. Transient Studies," Can. J. Chern. Eng., 60, 728 (1982) .

69. Kurylko, L. and Essenhigh, R.H., "Steady and Unsteady Combustion of Carbon," Fourteenth Symposium (International) on Combustion, p. 1375, The Combustion Institue, 1973.

70. Sotirches, S.V., Ph.D. Dissertation, University of Houston, Houston, TX, 1982.

71. Goblirsch, G.M. and Sondreal, E.A., "Fluidized Combustion of North Dakota Lignite," Presented at Lignite Symposium Grand Forks, North Dakota, 1977.

72. Patankar, S.V., Numerical Heat Transfer and Fluid Flow, Hemisphere Publishing Corporation, (1980).

73. Sotirchos, S.V. and Amundson, N.R., "Diffusion and Reaction in a Char Particle and in the Surrounding Gas Phase - A Continuous Model", Ind. Engr. Chern. Fund., 23, p. 191, (1984).

74. Howard, J.B., Williams, G.C. and Fine, D.H., 14th International Symposium on Combustion, The Combustion Institute, Pittsburgh, PA (1973).

75. Smith, I.W. and R.J. Tyler "Internal Burning of Pulverized Semianthracite: The Relation Between Particle Structure and Reactivity," Fuel, Vol. 51, (1972).

76. Dutta, S., Wen, C.Y. and Belt, R.J., Industrial Engineering Chemistry Process Design and Development (1977) .

77. Wen, C.Y. and Ishida, M., "Reaction Rate of Sulfur Dioxide With Particles Containing Calcium Oxide," Environmental Science and Technology, Vol. 7, No. 8, (1973) .

78 . Westmoreland, P.R., Gibson, J.B. and Harrison, D.P., "Comparative Kinetics of High Temperature Reaction Between H2S and Selected Metal Oxides," Environmental Science and Technology, Vol. 13, No. 5 (1979) .

79. Yang, R.T. and Chen, J.M., "Kinetics of Desulfurization of Hot Fuel Gas With Calcium Oxide. Reaction Between Carbonyl Sulfide and Calcium Oxide," Environmental Science andTechnology , Vol. 13, No. 5 (19 7 9) .

APPENDIX A

APPENDIX B

APPENDIX C

CALCULATION OF FILM THICKNESS

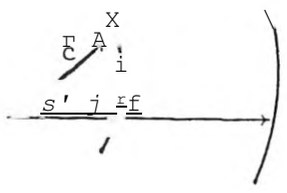

r_c: radius of char

r_f: radius of gas film

$$\frac{\partial}{\partial r}\left(r^2 k \frac{\partial T}{\partial r}\right) = 0$$

Integrate

$$k_F \frac{\partial T}{\partial r} 4 \pi r^2$$

Solve for C^

$$\int_{T_C}^{T_F} dT = \left[C_1 \left(-\frac{1}{r}\right) \right]_A^{r_f}$$

$$T_f - T_c = k \left(\quad \right)$$

$$C_1 = \frac{k(T_f - T_c)}{\left(\frac{1}{r_c} - \frac{1}{r_f}\right)}$$

Substitute C^ in equation 1 and r = r^

$$\left.\frac{\partial T}{\partial r}\right|_{r=r_c} = \frac{(T_f - T_c)}{\left(\frac{1}{r_c} - \frac{1}{r_f}\right)\left(\frac{1}{r_c}\right)}$$

$$\frac{h}{k} r_c = Nu = \frac{2}{1 - \frac{r_c}{r_f}}$$

$$-hA(T_c - T_f) = k A \left.\frac{\partial T}{\partial r}\right|_{r = r_c}$$

$$r_f = -\frac{Nu\, r_c}{2 - Nu}$$

$$-\frac{h}{k}(T_c - T_f) = \frac{(T_f - T_c)}{\left(\frac{1}{r_c} - \frac{1}{r_f}\right)\left(\frac{1}{r_c}\right)}$$

CALCULATION OF N AND ct

N_i = number of pores

r_P = radius of pores

r_C = radius of char

$a = r_P / r_C$

θ = Porosity = $\frac{\text{Pore volume}}{\text{Total volume}}$

For Conical Pores

Pore Volume = $N\ 1/3\ \pi\ r\ r_P^2\ r_C$

Total Volume = $4/3\ \pi r_C^3$

$$\theta = N\ 1/4\ (\theta A_c\ r^2$$

$$\boxed{N = \frac{4\Theta}{u^2}}$$

$$\frac{A}{\Theta} = \frac{\text{Pore Area}}{\text{Porosity}} = \frac{N\pi\ r_p \sqrt{r_p^2 + r_c^2}}{N\ 1/2\ (r_P / r_C)^2}$$

$$\frac{A}{\theta} = 4\pi' r_c\ /1^2 +/(-)\ .1^2\ \alpha$$

$$\boxed{\alpha = \frac{1}{\sqrt{\left(-\frac{1}{4\pi\ r_c^2}\ \frac{A}{\theta}\right) - 1}}}$$

```
C CHAR COMBUSTION MODEL
C
C
C ENTER CHAR RADIUS;RC(METER),BET AREA(M**2/KG),POROSITY ; PORE,
C ENTER DENSITY;DENSE(KG/M**3),VELOCITY ; U(M/SEC),VISCOSITY ; VIS(M**2/S)
C ENTER PRANDTL NUMBER;PRAN, NUMBER OF NODES ;N,PRESSURE ;P(ATM)
C
C
      REAL*B RR(101),T(101),Cl(101),C2(101),C3(101),DIFF1(101)
     X,DIFF2(101),DIFF3(101),TK(101),RH(101),RS(101),HRS(101),TT(101)
     X,BJ1(1O1),BJ2(1O1),BJ(101),DI(101),D2(101),D(101),PP(101),Q(101)
     X, RB (99), D3 (99), HRB (99), UC (99), C4 (99) , HC1 (99) , HC2 (99) , HC3 (99)
     X,NF1(101),NF2(101),NF3(101),CVE(101),CC3(101),UCC(101),TTT(101)
     X,TA(101),TAA(lOl),RM(101),C5(101),SREL(101),DIFF4(101)
      REAL NU
      WRITE(3,90)
   90 FORMAT(2OX,'CHAR MODEL',//,'XXXXXXXXXXXXXXXXXXXXXXXXXXXXXXXXXXXXXX
     XXXXXXXXXXXXXXXXXXXXXXXXXXXXXX')
      RC=0.5E-3
      BET=2.1D+3
      P0RE=0.35
      DENSE=9.0E+2
      U=2.0
      VIS=138.6E-6
      PRAN=0. 704
      N=50
      P=1.0
      HRH=5.64E+8
      CPG=39.77E+3
      PORA=.45
      TS=0.313
      CS=TS/2
C
C PROGRAM STARTS
      POROD=PORE
      R=0.08206
      PIE=3.141593
      A=BET*DENSE*4.O*PIE*(RC**3)/3.0
      DEN=1.0/(4.O*PIE*(RC**2))
      DEN1=(DEN*A/PORE)**2-1.0
      ALPHA=1.0/(DEN1**O. 5)
      RE=U*2.O*RC/VIS
      NU=2.0+0.6*(RE**0.5)*(PRAN**(0.3333))
      RF=NU*RC/(NU-2.0)
      DR=RF/N
      SRC=(RC+(DR/2))/DR
      NRC=SRC
      E=SRC-NRC
```

```
      IF(E.GT.O.5)NRC=NRC+1
      NA=NRC
      DR=RC/(NRC-O. 5)
      RF=N*DR
      RR(l)=0.0
      M=N+1
      DO 10 J=2,M
   10 RR(J)=(J-1)*DR
C
C GUESS TEMPERATURE PROFILE
C
      DO 40 1=1,N
   40 T(I)=1200
      T(N)=1100
      IP=7
C
C GUESS CONCENTRATION PROFILE
C
      DO 50 1=1,NRC
      Cl(I)=0.0
      C2(I)=0.0
   50 C3(I)=0.0
      DO 60 I=NRC,N
      Cl(I)=0.13*P/(R*T(I))
      C2(I)=0.036*P/(R*T(I))
   60 C3(I)=0.072*P/(R*T(I))
      JJJ=0
   81 CONTINUE
   47 CONTINUE
      NSP=1
      CALL DIFFS(RR,DR,NRC,NA,N,ALPHA,T,NSP,DIFF1)
      NSP=2
      CALL DIFFS(RR,DR,NRC,NA,N,ALPHA,T,NSP,DIFF2)
      NSP=3
      CALL DIFFS(RR,DR,NRC,NA,N,ALPHA,T,NSP,DIFF3)
      DO 45 1=1,N
   45 TTT(I)=T(I)
C
C CALCULATE 02 COEFFICIENTS
C
      JJ=O
      JN=0
   72 CONTINUE
      NN=0
   71 CONTINUE
      CALL RATEH(N,T,C1,RH)
      CALL RATES(NRC,NA,T,RS)
      M=N-1
      DO 70 1=1,M
```

```
      BJ1(I)=(DIFF1(I+1)*RR(I+1)**2)/DR
      BJ2(I)=(DIFF1(I)*RR(I)**2)/DR
      D1(I)=-0.5*C3(I)*RH(I)*(RR(I+1)**3bRR(I)**3)/3
      D2(I)=(O.5*RS(I)*(1+ALPHA**2)**O.5)*(RR(1+1)**2
     X-RR(I)**2)/ALPHA
      IF(I.EQ.NRC)D2(I)=O.5*D2(I)*PORE
      IF(I.EQ.NRC)D1(I)=D1(I)*(1+PORE)/2
      IF(I.EQ.NRC)BJ2(I)=PORE*BJ2(I)
      BJ(I)=BJ1(I)+BJ2(I)+D2(I)+UC(I+1)*RR(I+1)**2
      BJ2(I)=BJ2(I)+UC(I)*RR(I)**2
   70 D(I)=D1(I)
C
C CALCULATE NEW C1
C
      CALL TDMA(N,BJ,BJ1,BJ2,D,PP,Q,C1)
C
C CALCULATE CO COEFFICIENTS
C
      DO 78 1=1,M
      IF(C1(I).LT.1.OD-15)C1(I)=0.0
   78 CONTINUE
      CALL RATEH(N,T,C1,RH)
      CALL RATES(NRC,NA,T,RS)
      CALL RATEB(NRC,NA,T,RB)
      DO 75 1=1,M
      BJ1(I)=(DIFF3(I+1)*RR(1+1)**2)/DR
      BJ2(I)=(DIFF3(I)*RR(I)**2)/DR
      D2(I)=(RS(I)*C1(I)*(1+ALPHA**2)**O.5)*(RR(I+1)**2
     X-RR(I)**2)/ALPHA
      D3(I)=(2*RB(I)*C2(I)*(1+ALPHA**2)**0.5)*(RR(I+1)**2
     X-RR(I)**2)/ALPHA
      D1(I)=RH(I)*(RR(I+1)**3-RR(I)**3)/3
      IF(I.EQ.NRC)D2(I)=0.5*D2(I)*PORE
      IF(I.EQ.NRC)D3(I)=0.5*D3(I)*PORE
      IF(I.EQ.NRC)BJ2(I)=BJ2(I)*PORE
      IF(I.EQ.NRC)D1(I)=D1(I)*(1+PORE)/2
      BJ(I)=BJ1(I)+BJ2(I)+D1(I)+UC(I+1)*RR(I+1)**2
      BJ2(I)=BJ2(I)+UC(I)*RR(I)**2
   75 D(I)=D2(I)+D3(I)
C
C CALCULATE NEW C3
C
      DO 77 1=1,N
   77 CC3(I)=C3(I)
      CALL TDMA (N,BJ,BJI,BJ2,D,PP,Q,C3)
C
C CALCULATE CO2 COEFFICIENTS
C
```

```
      CALL RATEB(NRC,NA,T,RB)
      DO 83 1=1,M                    I
      BJ1(I)=(DIFF2(1+1)*RR(I+1)**2)/DR
      BJ2(I) =(DIFF2(I)*RR(I)**2)/DR
      Dl(I)=RH(I)*C3(I)*(RR(I+l)**3-RR(I)**3)/3
      D2 (I) + (RB(I)*(1+ALPHA**2)**O.5)*(RR(I+1)**2
     X-RR(I)**2)/ALPHA
      IF(I.EQ.NRC)D2(I)=O.5*D2(I)*PORE
      IF(I.EQ.NRC)BJ2(I)=BJ2(I)*PORE
      IF(I.EQ.NRC)Dl(I)=Dl(I)*(l+PORE)/2
      BJ(I)=BJ1(I)+BJ2(I)+D2(I)+UC(I+1)*RR(I+1)**2
      BJ2(I)=BJ2(I)+UC(I)*RR(I)**2
   83 D(I)=D1(I)
C
C CALCULATE NEW CO2
C
      CALL TDMA(N,BJ,BJ1,BJ2,D,PP,Q,C2)
      NN=NN+1
      IF(NN.GT.30)WRITE(3,102)IP
  102 FORMAT(3X,'SPECIES EQUATIONS HAVE EXCEEDED 20 LOOPS',13)
      IF(NN.GT.30)GO TO 74
      TOL=DABS (CC3 (NRO-C3 (NRC) )
      TOL=TOL*100000.
      IF(TOL.LT.2.0)GO TO 74
   74 CONTINUE
C
C CALCULATE N2 CONCENTRATION
C
      DO 79 1=1,N
   79 UCC(I)=UC(I)
      NT=NRC+1
      DO 91 I=NRC,N
   91 C4(I)=(P/(R*T(I)))-Cl(I)-C2(I)-C3(I)
      DO 92 I=NT,N
      UC(I)=DIFF1(I)*DLOG(C4(I)/C4(1-1))/DR
   92 CONTINUE
      JN=JN+1
      IF(UN.GT.20)WRITE(3,102)
      IF(JN.GT.20)G0 TO 76
      TOL=DABS(UCC(I)-UC(I))
      T0L=T0L*1000
      IF(TOL.LT.1.0)GO TO 76
      GO TO 72
   76 CONTINUE
      IP=IP+1
      IF(IP.EQ.4)IP=7
      IF(IP.EQ.1)C1(N)=.16*P/(R*T(N))
```

```
      IF(IP.EQ.2)C1(N)=.17*P/(R*T(N))
      IF(IP.EQ.3)C1(N)=.18*P/(R*T(N))
      IF(IP.EQ.4)C1(N)=.19*P/(R*T(N))
      IF(IP.EQ.5)C1(N)=.2*P/(R*T(N))
      IF(IP.EQ.6)C1(N)=.21*P/(R*T(N))
      NN=O
      JN=O
      IF(IP.LT.7)GO TO 71
C
C CALCULATE ENERGY COEFFICIENTS
C
      X=0.75
      T0L=0.0
      CALL RATEH(N,T,C1,RH)
      CALL RATES(NRC,NA,T,RS)
      CALL RATEB(NRC,NA,T,RB)
      CALL THERMK(N,NRC,NA,T,TK)
      CALL HEATS(NRC,T,HRS,HRB)
   93 CONTINUE
   98 CONTINUE
      DO 80 1=1,M
      IF(I.GE.NA)PORE=PORA
      IF(I.GT.NRC)PORE=1.0
      BJ1(I)=(TK(I+1)*RR(I+1)**2)/DR
      IF(I.EQ.1)BJ1(I)=1*BJ1(I)
      IF(I.EQ.l)BJ2(I)=0.0
      IF(I.EQ,1)GO TO 97
      BJ2(I)=(TK(I)*RR(I)**2)/DR
   97 Dl(I)=0.5*C3(I)*RH(I)*HRH*PORE*
     X(RR(I+1)**3-RR(I)**3)/3
      D2(I) =(-0.5*C1(I)*RS(I)*HRS(I)*PORE*(1+ALPHA**2)**O.5)
     X*(RR(I+1)**2-RR(I)**2)/ALPHA
      D3(I) =(RB(I)*C2(I)*HRB(I)*PORE*(1+ALPHA**2)**0.5)
     X*(RR(I+1)**2-RR(I)**2)/ALPHA
      RAD=T(NRC)**4-T(N)**4
      EM=0.9
      IF(NA.NE-NRC)EM=0.75
      RAD=EM*RAD*5.669E-8*RC**2
      IF(I.EQ.NRC)D2(I)=0.5*D2(I)
      IF(I.EQ.NRC)D3(I)=0.5*D3(I)
      IF(I.EQ.NRC)D3(I)=D3(I)+RAD
      BJ(I)=BJ1(I)+BJ2(I)
   80 D(I)=D1(I)+D2(I)+D3(I)
      PORE=PORED
      DO 94 I=NT,M
      NF1(I)=(C1(I-1)*UC(I)-DIFF1(I)*(C1(I)-C1(I-1))/DR)
      NF2(I)=(C2(I-1)*UC(I)-DIFF2(I)*(C2(I)-C2(I-1))/DR)
   94 NF3(I)=(C3(I-1)*UC(I)-DIFF3(I)*(C3(I)-C3(I-1))/DR)
```

```
      T(M)=T(N)
      DO 95 I=NT,M
   95 CVE(I)=(NF1(I)+NF2(I)+NF3(I))*CPG*(1.O-T(1)/T(1))**RR(I)**2
      DO 96 1=1,M
      BJ1(I)=BJ1(I)-CVE(I+1)
   96 BJ(I)=BJ(I)-CVE(I)
C
C
C CALCULATE NEW TEMPERATURES
C
C
      DO 84 1=1,M
   84 TT(I)=T(I)
      CALL TDMA(N,BJ,BJ1,BJ2,D,PP,Q,T)
      JJ=JJ+1
      IF(JJ.GT.40)G0 TO 88
  164 FORMAT(3X,F8.2)
      TOL=DABS(TT(NRC)-T(NRC))
      IF(JJ.EQ.1)DTOL=TOL
      IF(DTOL.LT.TOL)X=1.O5*X
      DO 31 1=1,M
      IF(DT0L.LT.T0L)T(I)=TA(I)*2.0
      IF(DTOL.LT.TOL)TT(I)=TAA(I)= 2.0
      TA(I)=T(I)
      TAA(I)=TT(I)
   31 T(I)=X*TT(I)+(1-X)*T(I)
      IF(DTOL.LT.TOL)TOL=TOL+1O.0
      DTOL=TOL
      IF(TOL.LT.2.O)GO TO 88
      GO TO 93
   88      CONTINUE
      JJJ=JJJ+1
      TOL=DABS(TTT(25)-T(25))
      IF(TOL.LT.1.0)GO TO 89
      IF(JJJ.GT.100)GO TO 89
      DO 46 1=1,N
   46 T(I)=0.80*TTT(I)+0.20*T(I)
      GO TO 81
   89      CONTINUE
C
C
C CALCULATE S-SPECIES COEFFICIENTS
C
      DO 300 1=1,N
      IF(Cl(I).GE.3.OE-8)NOX=I
      IF(Cl(I).GE.3.OE-8)GO TO 310
  300 CONTINUE
  310 CONTINUE
```

```
      NSP=4
      CALL DIFFS(RR,DR,NRC,NA,N,ALPHA,T,NSP,DIFF4)
      CALL RATEMi(NRC,NA,NOX,T,RM)
      DO 320 1=1,M
      BJ1(I)=(DIFF4(1+1)*RR(I+1)**2)/DR
      BJ2 (I) = (DIFF4 (I) *RR(I) **2)/DR
      D1(I)=((TS*RS(I)*C1(I)+CS*RB(I)*C2(I))*
     C(l+ALPHA**2)**0.5)*(RR(I+1)**2-RR(I)**2)/ALPHA
      D2(I)=(RM(I)*(l+ALPHA**2)**0.5)*(RR(I+l)**2
     C-RR(I)**2)/ALPHA
      IF(I.EQ.NRC)D2(I)=0.5*D2(I)*PORE
      IF(I.EQ.NRC)BJ2(I)=BJ2(I)*PORE
      IF(I.EQ.NRC)D1(I)=D1(I)*0.5*PORE
      BJ(I)=BJ1(I)+BJ2(I)+D2(I)+UC(1+1)*RR(1+1)**2
      BJ2(I)=BJ2(I)+UC(I)*RR(I)**2
  320 D(I)=D1(I)
C
C CALCUALTE NEW S-SPECIES
C
      CALL TDMA(N,BJ,BJ1,BJ2,D,PP,Q,C5)
      DO 330 1=1,M
      RM(I)=RM(I)*C5(I)
      RM(I)=RM(I)*4*PIE*PORE*((1+ALPHA**2)**0.5)
     C*RR(I+1)**2-RR(I)**2)/ALPHA
      SREL(I)=TS*RS(I)*C1(I)+CS*RB(I)*C2(I)
      SREL(I)=SREL(I)*4*PIE*PORE*((1+ALPHA**2)**0.5)
     C*(RR(I+1)**2-RR(I)**2)/ALPHA
      RMM=RM(I)+RMM
      SSR=SREL(I)+SSR
  330 CONTINUE
      FCAP=RMM/SSR
C CALCULATE CO FLUX RATIO
      COR=C3(M)*DIFF3(M)/(C3(M)*DIFF3(M)+C2(M)*DIFF2(M))
C
C WRITE STATEMENT SECTION
C
      WRITE(3,104)JJJ,TOL,COR
  104 FORMAT(3X,'JJJ=',I3,2X,'TOL=',F5.2,2X,'COR=',F5.3)
      WRITE(3,100)RC,BET,PORE,DENSE,U
  100 FORMAT(3X,' RC= ',E7.2,2X,'BET=',E7.2,2X,'PORE=',F4.2,
     X2X,'DENSE=',E7.2,2X,'U=',F4.2)
  150 FORMAT(3X,'VIS=',E11.5,2X,'PR=',F6.4,2X,'N=',12,2X,'PRESSURE^
     X,F4.2)
      WRITE(3,160)ALPHA,RE,NU,RF,DR
  160 FORMAT(3X,'ALPHA=T,E8.3,2X,'RE=',F7.3,2X,'NU=',F5.3,2X
     X,'RF=',E9.4,2X,'DR=',E9.4)
      WRITE(3,170)NRC,NA,NOX,PORA,TS,FCAP
```

```
  170 FORMAT(3X,'NRC=',12,2X,'NA=',12,2X,'NOX=',I2,2X,'PORA=',F4.2,2X
     C, 'TS=',F6.4,2X,'FCAP=',E10.4)
      IVRITE (3,180)
  18 O FORMAT ( ’ XXXXXXXXXXXXXXXXXXXXXXXXXXXXXXXXXXXXXXXXXXXXXXXXXXXXXXX
     xxxxxxxxxxx',///)
      WRITE(3,185)
  185 FORMAT(2X,’NODE',5X,'TEMP',6X,'02 CONC',6X,'CO2 C0NC’,6X,’C0 CONC’
     X,6X,’S CONC’,//)
      DO 65 1=1,N
      IVRITE (3,190) I, TTT (I) , Cl (I) ,C2(I) ,C3(I) ,C5(I)
   65 CONTINUE
      IVRITE (3,340)
  340 FORMAT(//,2X,'NODE',5X,'TEMP',6X,'02 MOL%’,6X,’CO2 MOL%’,
     X6X,'CO MOL%’,6X,’S MOL%’,//)
      DO 67 1=1,N
      Cl(I)=Cl(I)*R*T(I)*100
      C2(I)=C2(I)*R*T(I)*100
      C3(I)=C3(I)*R*T(I)*100
      C4(I)=C4(I)*R*T(I)*100
      C5(I)=C5(I)*R*T(I)*100
      WRITE(3,190)I,T(I),C1(I),C2(I),C3(I),C5(I)
   67 CONTINUE
  190 FORMAT (3X, 12,3X, F8.2,6X, E10. 4, 3X, E10. 4 , 3X, E10. 4 , 3X, E10. 4 )
      WRITE(3,201)
  201 FORMAT(///,2X,’NODE’,5X,'DIFF 02’,6X,'DIFF CO2’,6X,’DIFF CO’,
     X6X,’DIFF S',//)
      DO 200 1=1,N
      WRITE(3,210)I,DIFF1(I),DIFF2(I),DIFF3(I),DIFF4(I)
  200 CONTINUE
  210 FORMAT (3X, 12, 3X, E10. 4,5X, E10.4,5X, E10. 4,5X, E10. 4 )
      IVRITE (3,220)
      DO 230 1=1,N
  220 FORMAT(///,2X,'NODE',5X,'THERMK',5X,'RATEM',9X,'S-REL')
  230 WRITE(3,240)I,TK(I),RM(I),SREL(I)
  240 FORMAT (3X, 12,4X, E10. 4,4X, E10. 4,4X, E10. 4)
      STOP
      END
C
C
C  SUBROUTINE  FOR  THERMAL  CONDUCTIVITIES
C
      SUBROUTINE THERMK(N,NRC,NA,T,TK)
      REAL*8 T(N),TK(N)
C TK(J/M*K*SEC)
      DO 10 1=1,NRC
   10 TK(I)=.157
      IF(NA.EQ.NRC)GO TO 16
      DO 15 I=NA,NRC
```

```
   15 TK(I)=0.7
   16 CONTINUE
      NNRC=NRC+1
      DO 20 I=NNRC,N
   20 TK(I)=2.627E-4*(0.5*(T(I-D+T(I))))**0.8
      RETURN
      END
C
C
C SUBROUTINE FOR DIFFUSIVITIES
C
      SUBROUTINE DIFFS(RR,DR,NRC,NA,N,ALPHA,T,NSP,DIFF)
      REAL*8 RR(N),T(N),DIFF(N)
C DIFF(M**2/SEC)
      IF(NSP.EQ.1)WM=32.0
      IF(NSP.EQ.2)WM=44.0
      IF(NSP.EQ.3)WM=28.0
      IF(NSP.EQ.4)WM=34.0
      RPA=2.0E-8
      DO 15 1=1,NRC
      RP=RR(I)*ALPHA
      IF(NA.EQ.NRC)GO TO 14
      IF(I.GE.NA)RR=RPA
   14     CONTINUE
   15 DIFF(I)=RP*97OO.0*(0.5*(T(I-1)+T(I))/WM)**0.5/100
      NNRC=NRC+1
      IF(NSP.EQ.2)GO TO 16
      IF(NSP.EQ.4)G0 TO 26
      DO 20 I=NNRC,N
   20 DIFF(I)=5.123E-9*(0.5*(T(I-l)+T(I)))**1.5
      GO TO 21
   16     DO 22 I=NNRC,N
   22 DIFF(I)=4.211E-9*(0.5*(T(I-l)+T(I)))**1.5
      GO TO 21
   26     DO 28 I=NNRC,N
   28 DIFF(I)=3.538E-9*(0.5*(T(I-1)+T(I)))**1.5
   21 CONTINUE
      RETURN
      END
C
C
C SUBROUTINE FOR HOMOGENEOUS REACTION RATE
                PER MOLE CO
C
      SUBROUTINE RATEH(N,T,C1,RH)
      REALES T(N),C1(N),RH(N)
      DO 10 1=1,N
      RKH=(3.04E+9)*DEXP(-15098/T(I))
```

```
      IF(Cl(I).LT.1.OE-15)Cl(I)=0.O
   IO RH(I)=RKH*C1(I)**O.5
      RETURN
      END

C
C
C SUBROUTINE FOR HETEROGENEOUS REACTION RATE CONSTANT
                PER MOLE CARBON
      SUBROUTINE RATES(NRC,NA,T,RS)
      REAL*8 T(NRC),RS(NRC)
      CC=0.5
      DO 10 1=1,NRC
   10 RS(I)=CC*(3.76*T(I))*DEXP(-20131/T(I))
      IF(NA.EQ.NRC)GO TO 16
      DO 20 I=NA,NRC
   20 RS(I)=0.0
   16 CONTINUE
      RETURN
      END
C
C
C SUBROUTINE FOR BOUDOUARD REACTION
              PER MOLE CARBON
C
      SUBROUTINE RATEB(NRC,NA,T,RB)
      REAL*8 T(NRC),RB(NRC)
      CC=0.5
      DO 10 1=1,NRC
   10 RB (I)=CC*1.47E+5*DEXP (-29844/T' (I) )
      IF(NA.EQ.NRC)GO TO 16
      DO 20 I=NA,NRC
   20 RB(I)=0.0
   16 CONTINUE
      RETURN
      END
C
C
C SUBROUTINE FOR SULFUR RETENTION REACTION RATE
C
C
      SUBROUTINE RATEM(NRC,NA,NOX,T,RM)
      REAL*8 T(NRC),RM(NRC)
      F=1.0
      CAO=.O451/F
      CAOO=.0451/F
      DO 10 1=1, NOX
      IF(NA.EQ.NRC)GO TO 5
```

```
      IF(I.GE.NA)CAO=CAOO
    5 CONTINUE
   10 RM(I)=CAO*(3.732E-4)*DEXP(-2579./T(I))
      DO 20 I=NOX,NRC
      IF(NA.EQ.NRC)GO TO 15
      IF(I.GE.NA)CAO=CAOO
   15 CONTINUE
   20 RM(I)=CAO*(2.386)*DEXP(-8807./T(I))
      RETURN
      END
C
C
C  SUBROUTINE  FOR  HETEROGENEOUS  HEAT  RELEASE
C
      SUBROUTINE HEATS(NRC,T,HRS,HRB)
      REAL*8 T(NRC),HRS(NRC),HRB(NRC)
      DO 10 1=1,NRC
      H=2423.8+5.632*T(I)-9.45E-3*T(I)**2+7.4E-7*T(I)**3
     X-(9.782E+5)/T(I)
      Hl=H*1.0E+3
   10 HRS(I)=Hl-2.21E+8
      DO 20 1=1,NRC
      H=-1605+16.54*T(I)-2.026E-2*T(I)**2+4.397E-6*T(I)**3
     X-(4.89E+5)/T(I)
      Hl=H*1.0E+3
   20 HRB(I)=H1+1.725E+8
      RETURN
      END
C
C TRIDIAGONAL MATRIX SOLUTION
C
      SUBROUTINE TDMA(N,BJ,BJ1,BJ2,D,PP,Q,Cl)
      REAL*8 BJ(N),BJ1(N),BJ2(N),D(N),C1(N),PP(N),Q(N)
      M=N-1
      PP(N)=0.0
      Q(N)=C1(N)
      DO 10 J=1,M
      I=N-J
      PP(I)=BJ2(I)/(BJ(I)-BJ1(I)*PP(I+1))
      Q(I)=(D(I)+BJ1(I)*Q(I+1))/(BJ(I)-BJ1(I)*PP(1+1))
      IF(Q(I).LT.1.0D-20)Q(I)=0.0
   10 CONTINUE
      C1(1)=Q(1)
      DO 20 1=2,M
   20 C1(I)=PP(I)*C1(I-1)+Q(I)
      RETURN
      END
```

BIOGRAPHICAL SKETCH OF THE AUTHOR

Frank Willis Cox, son of Frank Edward Cox and Walterine Hebert Cox, was born on August 29, 1959, in Biloxi, Mississippi.

He attended Stone County High School, in Wiggins, Mississippi, and graduated in May, 1978. He received the Bachelor of Science degree in Chemical Engineering in December, 1981, at the University of Mississippi. He graduated Magna Cum Laude.

He worked for Exxon Chemical Company until July, 1982. At that time he was accepted into the Graduate School at the University of Mississippi.

Frank is a member of Tau Beta Pi, Phi Kappa Phi, and the American Institute of Chemical Engineering, and the Division of Fuel Chemistry in the American Chemical Society.